Composites: Part A 209 (2026) 109970

Contents lists available at ScienceDirect

Composites Part A

journal homepage: www.elsevier.com/locate/compositesa

Phenolic-modified bacterial nanocellulose composites with antimicrobial and antioxidant activity for implantable biomaterials

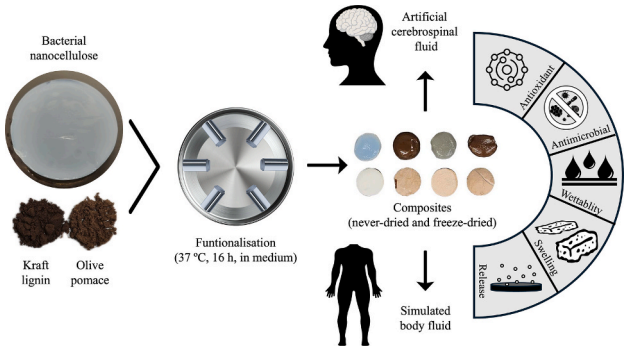
Liliana Melro [a,1], Cátia Alves [a,1], Marta Fernandes [a], Rui D.V. Fernandes [a], Adriana Pereira [a], Diego Moldes [b], Ana Cristina Rodrigues [c,d], Vitor Sencadas [e], Bogdana Mitu [f], Veronica Satulu [f], José Lourenço [g], Giorgio Pace [g], Luis A. Martins [h], José Luis Gómez Ribelles [h,i], António J. Salgado [j,k], Jorge Padrão [a], Andrea Zille [a,*]

[a] Centre for Textile Science and Technology (2C2T), Department of Textile Engineering, University of Minho, Campus of Azurém, 4800-058 Guimarães, Portugal
[b] CINTECX, Department of Chemical Engineering, University of Vigo, Campus As Lagoas-Marcosende, Vigo 36310, Spain
[c] Centre of Biological Engineering (CEB), Campus of Gualtar, University of Minho, 4710-057 Braga, Portugal
[d] LABBELS – Associate Laboratory, Braga, Portugal
[e] CICECO – Aveiro Institute of Materials, Department of Materials and Ceramics Engineering, University of Aveiro 3810-164 Aveiro, Portugal
[f] National Institute for Lasers, Plasma and Radiation Physics, 077125 Măgurele, Romania
[g] Centre of Molecular and Environmental Biology (CBMA)/Aquatic Research Network (ARNET) Associate Laboratory, University of Minho, Campus de Gualtar, 4710-057 Braga, Portugal
[h] Center for Biomaterials and Tissue Engineering, Universitat Politecnica de Valencia 46022 Valencia, Spain
[i] CIBER de Bioingenieria, Biomateriales y Nanomedicina, Instituto de Salud Carlos III, 46071 Valencia, Spain
[j] Life and Health Sciences Research Institute (ICVS), School of Medicine, University of Minho, Campus de Gualtar, 4710-057 Braga, Portugal
[k] ICVS/3B's – PT Government Associate Laboratory, Braga/Guimarães, Portugal

HIGHLIGHTS

- Bacterial nanocellulose (BNC) composites for cranium and postcranium bioimplants.
- Valorisation of Kraft lignin (KL) and olive pomace (OP) subproducts.
- KL and OP biological activity without synthetic additives.
- Application-specific characterisation of biocomposites.

GRAPHICAL ABSTRACT



ARTICLE INFO

Keywords:
Bacterial Nanocellulose
Kraft Lignin

ABSTRACT

Kraft lignin (KL) and olive pomace (OP) are macromolecules abundant in phenolic compounds with significant potential in biomedical applications. Bacterial nanocellulose (BNC) is a non-toxic biodegradable biopolymer that has been demonstrated as a promising alternative for implantable materials. In this work, KL and OP extracts

* Corresponding author.
E-mail address: azille@2c2t.uminho.pt (A. Zille).
[1] Authors contributed equally to the manuscript.

https://doi.org/10.1016/j.compositesa.2026.109970
Received 26 March 2026; Received in revised form 12 May 2026; Accepted 25 May 2026
Available online 28 May 2026
1359-835X/© 2026 The Authors. Published by Elsevier Ltd. This is an open access article under the CC BY license (http://creativecommons.org/licenses/by/4.0/).

Olive Pomace
Antimicrobial Activity
Antioxidant Efficiency
Biomedical Application

were incorporated into both freeze-dried and never-dried BNC samples, with thicknesses of 1 and 3 mm. To comprehend the incorporation of the KL and OP extracts onto the porous membrane, the pore size of untreated BNC was measured by porometry (197 nm). The size of KL and OP particles was below 0.3 μm^2 as observed using Scanning Transmission Electron Microscopy (SEM). The modification of BNC with these active agents was carried out through an exhaustion process, and the resulting composites were characterised using various analyses, including morphological, chemical, physical, thermal, and biological assessments. Considering the use of cranium and postcranium implants, all BNC composites demonstrated a desirable residual release, which aids to minimise cytotoxicity, while preserving biological properties. The composites exhibited antimicrobial activity, particularly the OP-based composites, showing greater effectiveness against *Staphylococcus aureus* (with a 3 mm freeze-dried sample, obtaining 2.5 log reduction) and MS2 (both 1 and 3 mm never-dried samples, achieving 4.2 log reduction). In addition, the antioxidant properties were confirmed, reaching a maximum of 77 and 72% for freeze-dried BNC/OP and BNC/KL, respectively. Overall, these exploratory findings highlight a strong potential for bio-based implant applications.

1. Introduction

Bioimplants are increasingly warranted due to clinical breakthroughs and the ageing population. These are intended to support, fix, or improve the functions of human tissues, and may encompass brain/neural, bone/cartilage, dental, and abdominal support applications [1]. Implanted devices must meet specific criteria, namely possess a desired host response and integrate with surrounding tissues. Good handling properties for friendly surgical implantation, as well as the ability to withstand sterilising procedures, are also required. In addition, depending on their application, they demonstrate sufficient mechanical properties [2]. Nanocellulose materials, namely cellulose nanocrystals, cellulose nanofibres, and bacterial nanocellulose, present barrier properties, non-toxicity, and can be easily functionalised. They have been widely studied for biomedical applications, namely implants, drug delivery, and scaffolds in tissue engineering [3]. Bacterial nanocellulose (BNC) is a promising natural biopolymer synthesised by certain bacterial species as an exopolysaccharide of ß-D glucopyranose. It has strong mechanical, barrier, and permeability properties, being biochemically inert and highly biocompatible as proven by in vitro, ex ovo, and in vivo investigations [4,5]. The ease with which BNC can be sterilised and the fact that it is not degraded by the human body make it durable and suitable for implants [2]. Antimicrobial activity and increased adhesion in BNC can only be achieved through functionalisation [6]. Kraft lignin (KL) and bagasse extracted from olive pomace (OP) are two potential biological compounds for BNC modification for prospective application as a bioimplant in the cranium and postcranium.

Lignin is a natural phenolic polymer obtained primarily from wood and is the most abundant biopolymer in nature after cellulose, accounting for 18–35% of the wood dry matter [7]. With an amorphous structure, rich in aromatic alcohols, lignin is composed mainly of three basic phenylpropanolic monomers: *p*-coumaryl (H), coniferyl (G), and sinapyl (S) (Fig. 1a) [8]. Several extraction processes can be used to obtain pure lignin (sulphite, Kraft, organosolv, and soda processes) [9]. In the present work, lignin was extracted by Kraft process, the most common method, responsible for 85% of lignin extraction [10,11]. One of the main disadvantages of this compound is its reduced solubility in water, due to the extremely alkaline conditions applied during the extraction process [11]. Some of lignin's interesting properties are its satisfactory stiffness, good thermal stability, and resistance to moisture and fungi [12,13]. Ultraviolet (UV) protection, antioxidant, antimicrobial, and flame-retardant properties may be ascribed due to functional groups on the benzene ring present in lignin molecules, such as methoxy ($-OCH_3$), phenolic hydroxyl (Ar–OH), aliphatic hydroxyl (Alk–OH), and side-chain carbonyl (C=O) [14]. These properties make lignin a promising candidate for potential applications in drug delivery, tissue engineering, wound dressing, pharmaceutics, and medical devices [15]. The inclusion of lignin within a BNC matrix generates a fully bio-based composite encompassing the excellent properties of both components, improved water and gas barrier properties [16], biocide activities [17], and UV-absorbing characteristics [18].

OP is a semi-solid to semi-liquid by-product obtained from the olive's skin (10–11% (w/w)), core (42–54% (w/w)), and pulp (21–33% (w/w)) [19] and constitutes over 35% of the total weight of processed olives [20]. The general composition of OP is similar, depending on the olive cultivar, culture conditions or production process [21]. It is primarily composed of cellulose, hemicellulose, lignin, proteins, phenolic compounds (*p*-coumaric acid, tyrosol, hydroxytyrosol) (Fig. 1b), sugars, lipids, and mineral salts (potassium, calcium, and sodium), and has an acidic pH. As a result of the large number of phenolic compounds in its

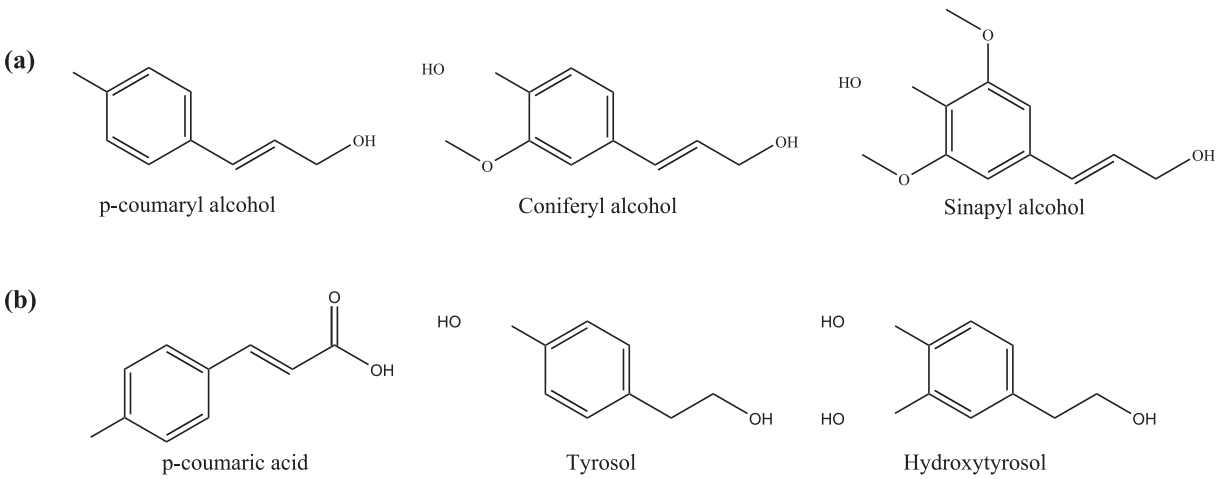


Fig. 1. Phenolic compounds of (a) KL (primary lignin alcohol monomers: *p*-coumaryl, coniferyl, and sinapyl) and (b) OP (*p*-coumaric acid, tyrosol, and hydroxytyrosol) [21,22].

composition, OP has antioxidant activity and antimicrobial properties. The phenol content is typically higher when OP is extracted by a two-phase centrifugation process [21].

Considering the intended application of the present study for cranial and postcranial bioimplants, it is important to endow BNC with biological properties. In this exploratory study, BNC was modified with KL and OP extracts to create a fully bio-based composite able to retain the structural integrity of BNC while introducing essential antimicrobial and antioxidant properties. Therefore, this hypothesis highlights the following key advancements over previous literature: (i) synergistic functionalization – since literature states the excellent mechanical strength and non-cytotoxicity of BNC [5,23], this study proposes that the integration of KL and OP extracts may provide biological activity in the absence of synthetic additives; (ii) subproduct valorisation – the study introduces a novel environmental and biomedical intersection by utilizing Kraft process by-products and olive mill waste to enhance medical-grade biopolymers, offering a sustainable alternative to traditional implant functionalization methods; and (iii) application-specific optimisation – unlike general BNC studies, this research differentiates by focusing the target site of the implant through the modification of the physical state of the BNC, hypothesizing that freeze-dried BNC is superior for cranial adaptability (nerve contact) whereas never-dried BNC is superior for load-bearing body applications. To follow these hypotheses, BNC was modified with KL and OP, individually, or combined to evaluate a potential synergistic effect. The exhaustion process was selected due to a more homogeneous incorporation without changes to the pristine structure of BNC. Despite being a preliminary work, their use in cranium applications was simulated by conducting the physical assays in artificial cerebrospinal fluid (aCSF), while simulated body fluid (SBF) was chosen for body-intended applications. Freeze-dried BNC is of particular interest for cranial use, due to its sponge-like structure, which allows for better adaptability and direct contact with nerves. In contrast, never-dried BNC, is preferred for body-intended applications given the expected superior mechanical properties. Both physical states of the modified BNC and different thicknesses (1 and 3 mm) were tested regarding morphological, physical, thermal, antimicrobial, and antioxidant properties.

2. Results and Discussion

Materials and methods of all performed assays are available in Supporting Information.

2.1. Media selection for the optimisation of KL and OP dispersions

The biopolymers' solubility/dispersibility behaviour across different media, including water, NaOH, BRB, and PBS (Table S1) was studied by optical microscopy. Fig. 2a provides a comparative analysis of their dispersion profiles in each medium. The biopolymers remained insoluble in water, with more KL and OP agglomerates than in other media. Nearly complete solubilisation was achieved in NaOH due to the alkaline pH (9–10) of the solvent, which enhances lignin solubility [11]. However, the cytotoxic nature of NaOH limits its suitability for implant applications [24]. The results obtained for both buffers, BRB and PBS (pH 7.0 and 7.4, respectively), were comparable. Nonetheless, BRB presents a considerable limitation due to its composition, which includes formic acid, a highly toxic compound, representing the simplest form of an organic acid [25,26]. Thus, PBS and water were selected for BNC

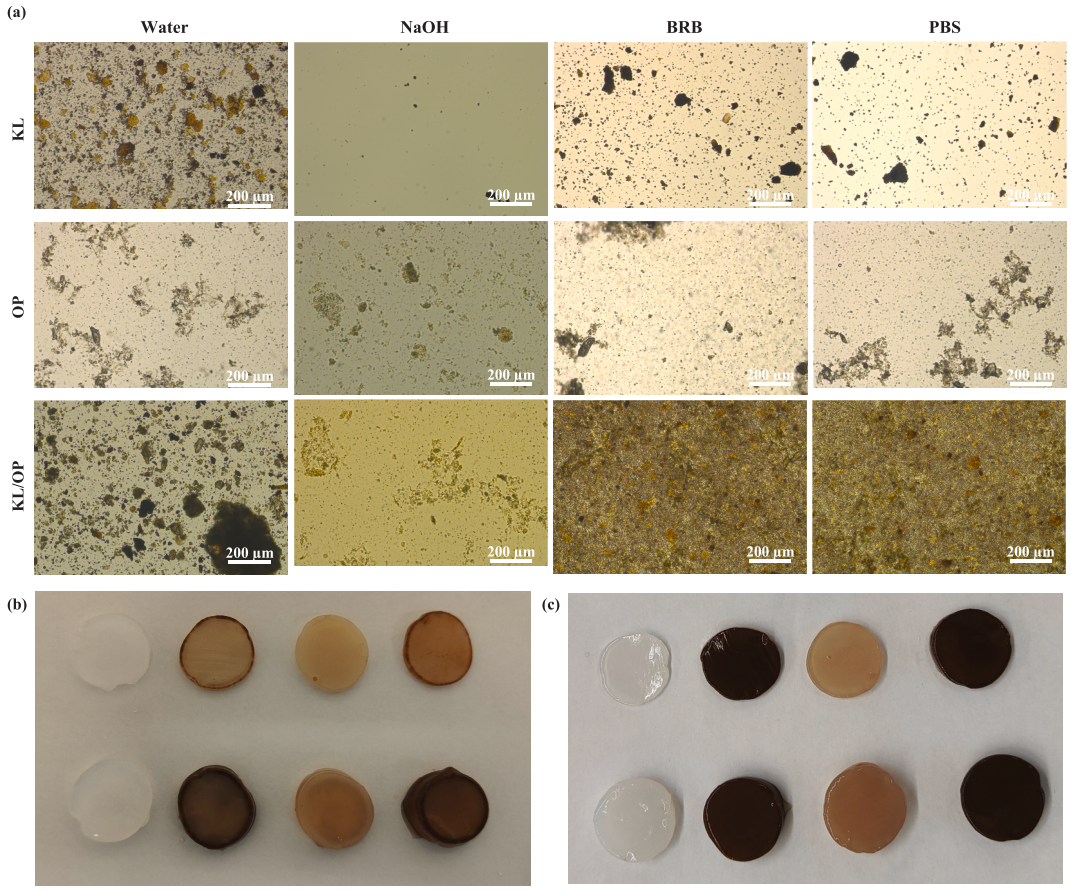


Fig. 2. Microscopic images of the KL, OP, and KL/OP suspensions in water, NaOH, BRB, and PBS (a); BNC membranes prepared using water (b) and PBS (c) as dispersion media of the biopolymers. The first row displays composites with a thickness of 1 mm, while the second row shows those with a thickness of 3 mm. From left to right, the samples are identified as pristine BNC, BNC/KL, BNC/OP, and BNC/KL/OP.

modification (Fig. 2a).

Fig. 2b, c highlights the modified samples, showing that the compounds display considerably improved dispersibility in PBS. This enhanced dispersibility was indicated by a more pronounced penetration of KL and OP into the BNC structure than in the water-treated samples. The PBS modified samples show higher colour intensity and a more uniform distribution of the macromolecules, highlighting the superior performance of PBS as a dispersing medium in promoting effective modification. The primary objective was to assess each medium's compatibility and efficiency in facilitating the incorporation of KL and OP into the BNC matrix. This evaluation was crucial for determining the medium to ensure the most effective modification and to enhance the material's properties for its intended biomedical use. Attending the application, PBS was selected as the dispersing medium due to its biocompatibility with human body fluids and its non-toxic nature [27].

2.2. Physicochemical and biological characterisation

2.2.1. Size, structure and morphology of the extracts and BNC composites

As observed in the STEM images in Fig. 3a–c (left), a heterogeneous particle distribution was obtained for both extracts and their mixture, in particular for KL particles. The images also suggest the presence of larger particles in KL in comparison with OP and KL/OP. This was corroborated by the histograms in Fig. 3a–c (right), which indicate that complete dispersion was not achieved, as mentioned in Fig. 2a. In general, OP particles predominantly exhibited areas inferior to 0.3 μm^2 (approximately 93%). The prevalence of KL and KL/OP particles lower than 0.3 μm^2 was nearly 89 and 86%, respectively. Although biopolymers were slightly present on the BNC surface, their particle size was sufficiently

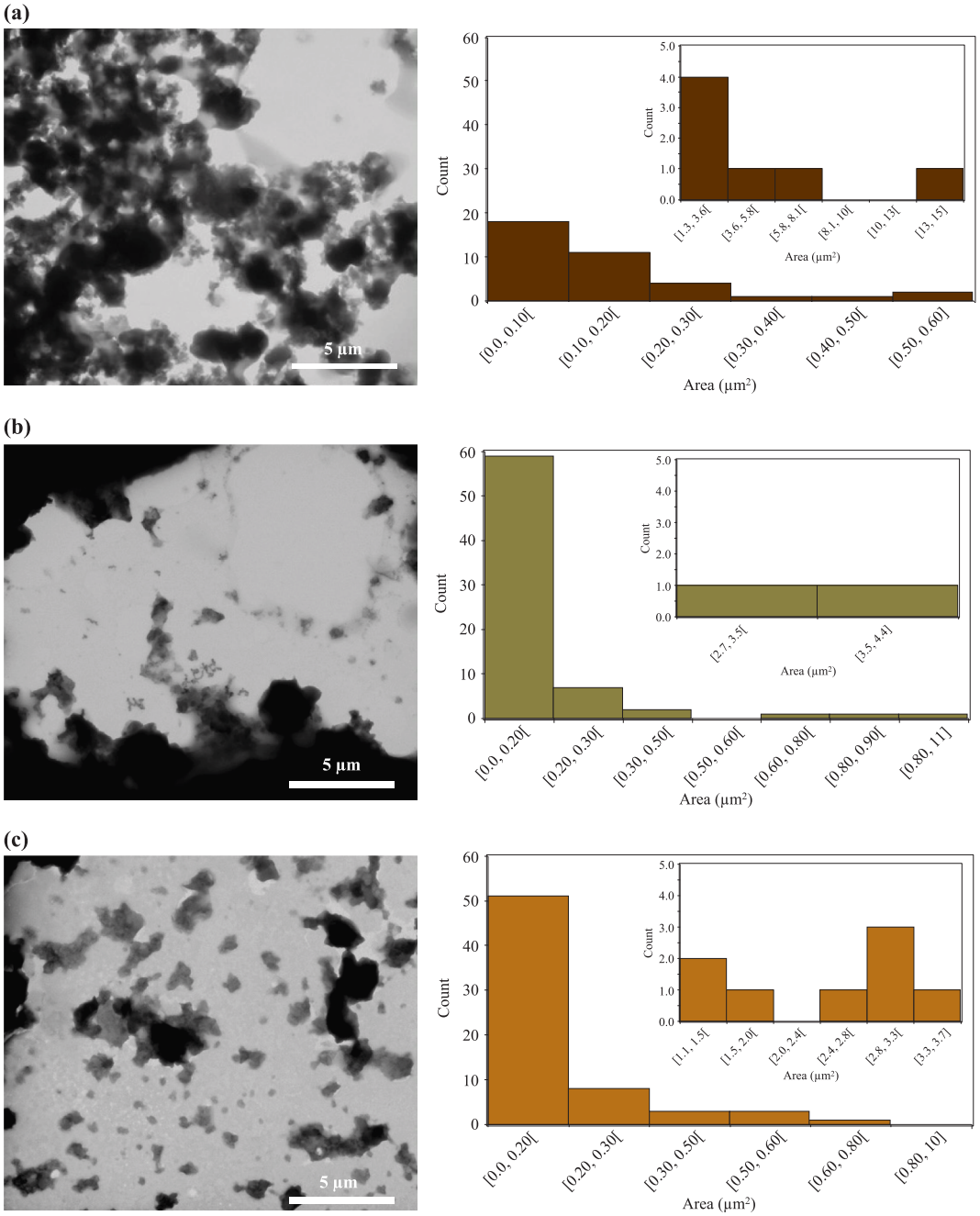


Fig. 3. STEM images and area particle analysis of (a) KL, (b) OP, and (c) KL/OP.

large to hinder their incorporation into the internal layers of BNC.

A three-dimensional (3D) network typical of BNC with several overlapping is noticeable in both the Cryo-FESEM images in Fig. 4a–f and the representative cross-section (Fig. 4a–c) and surface images of the freeze-dried membranes (Fig. 4d–f). The random orientation of nanofibrils characterises this network, classifying the BNC as a nonwoven structure [28]. The fibre diameter of BNC is dependent on the producing species. According to the histogram determined from Cryo-FESEM images (Fig. 4g), fibre diameter between 149–230 nm was determined for *K. hansenii*. This is in agreement with the literature for this specific bacterium species, where diameters between 70–150 nm [29] and 160 nm [30] have been reported. A very porous structure with a high surface area was observed, as is characteristic of the type of nanocellulose under study, with or without the incorporation of KL and OP. The aggregation of these macromolecules on the BNC surface suggests a potential electrostatic interaction between them (Fig. 4o), which is likely influenced by the lignin content. The absence of aggregation only observed in the OP surface (Fig. 4n) further indicates that this phenomenon may be attributed explicitly to KL (Fig. 4m). Despite the lack of evidence of KL and OP presence in the cross-sectional images of BNC nanofibers (Fig. 4i–k), the pore size reduction evaluated by capillary flow porometry in section 2.2.3, suggests the diffusion of these particles through the BNC matrix. Furthermore, a more pronounced collapse of the BNC structure can be attributed to the particle size of KL, as illustrated in Fig. 4m, o. However, OP did not induce any structural modification in the BNC [31]. Furthermore, the surface SEM images display fewer biopolymer particles on the BNC surface (Fig. 4m, o).

2.2.2. Crystalline structure

The XRD pattern of the purified BNC exhibited characteristic reflections of native Cellulose I (Fig. 5) [32], with a prominent peak at $2\theta \approx 22.8^{\circ}$ corresponding to the (200) lattice plane. The calculated CI was found to be 94%, a value rather similar to what has been reported in the literature for freeze-dried BNC [33]. This exceptional crystallinity confirms the high purity of the biosynthesized nanocellulose and the efficacy of the alkaline purification process in removing non-cellulosic bacterial biomass.

2.2.3. Pore size

The pore size was evaluated using the capillary flow porometry technique (Table 1). The BNC exhibited an average pore size of 197 nm (0.031 μm^2), classifying it as a macroporous structure, and this result aligns with previously reported literature, indicating a pore size range of approximately 0.0003–78.5 μm^2 [34]. Differences within this range may result from various factors, including the microbial strain responsible for production, the culture medium type of carbon source, and the drying method applied [35,36]. The tortuous nature of BNC constrains the continuous diffusion of macromolecules. As confirmed by SEM analysis (Fig. 4i–k), most of these particles cannot penetrate the 3D network, given that the fraction of particles smaller than 0.043 μm^2 (233 nm) is only 11% for KL, 56% for OP, and 37% for KL/OP. Consequently, the low concentration of small KL particles, result in no considerable reduction in pore size. Differently, OP particles led to a drastic pore size reduction, from 0.031 μm^2 (197 nm) to 0.0017 μm^2 (46 nm), due to the higher percentage of small OP particles effectively filled the bulk void spaces. For the KL/OP combination, the pore reduction was intermediate, likely due to the initial higher ratio of KL (2 wt%) compared to OP (1 wt%). This may suggest that the larger KL particles block the superficial pores, hindering the diffusion of OP particles into the BNC.

2.2.4. Surface area and adsorption isotherms

BET surface area and N_2 adsorption–desorption isotherms were performed to gain insights about the effect of the OP and KL on BNC surface area (Fig. 6a–e). It was observed that, for all samples, the adsorption/desorption curves overlapped in the region $0 < P/P_o < 0.5$, suggesting the presence of micropores with monolayer adsorption [37]. Further, a sudden increase was observed for $P/P_o < 0.9$, and did not attain a stable status even at $P/P_0 = 1$, indicating that the N_2 gas trapped was due to capillary condensation of mesopores or macropores, at a relative pressure lower than its saturation pressure, and is a characteristic of slit-shaped pores [38].The BET surface area of pristine BNC was found to be 20.49 and 26.69 $m^2.g^{-1}$, for 1 and 3 mm thicknesses, respectively (Fig. 6a), aligning with common values reported in the literature (comprised between 20 and 200 $m^2.g^{-1}$) [39–42]. The differences in BET surface area values can be attributed to the bacterial strain used for production and the post-treatment of the membranes, including the drying method. A study by Adepu et al. demonstrated that the surface area was higher in freeze-dried samples compared to oven-dried samples due to structural collapse during thermal drying [36]. The higher N_2 adsorption observed in the thicker composites suggests increased surface accessibility than in the 1 mm composites. This result may be associated with differences in a 3D network, potentially enhancing accessibility of micro- and mesopores [39]. Upon incorporating KL (BNC/KL), a reduction in BET surface area was observed regardless of composite thickness. This decline can be attributed to the decreased availability of surface area as KL deposition on the BNC surface effectively blocked adsorption sites. For BNC/OP and BNC/KL/OP composites, surface area values remained comparable to those of the non-functionalised 1 mm sample. However, a slight reduction in BET surface area was noted for the 3 mm composites. This suggests that KL deposition on thicker samples may produce a more uniform coating, leading to a slightly diminished accessible surface area.

2.2.5. Chemical structure of the extracts and composites

The transmittance spectra of FTIR analyses are illustrated in Fig. 7. The characteristic band of BNC between 3400–3200 cm^{-1} that corresponds to the O–H stretching vibrations present in the pyranose ring are seemingly unchanged in the spectra of the nanocomposites [43]. An exception occurs for the KL/OP composite that presents a broader band, more similar to the KL and OP powders. This suggests that the peak may have been masked due to the higher phenol content of the KL and OP. The characteristic small absorption bands at 2916 and 2850 cm^{-1} present in the BNC spectrum are attributed to C–H asymmetric and symmetric stretching vibrations of methylene ($–CH_2–$) groups in the cellulose structure. In contrast, the OP spectrum provides two better-defined peaks, due to higher aliphatic content, at 2924 and 2853 cm^{-1}, which are due to asymmetric and symmetric C–H stretching vibrations of methylene ($–CH_2–$) groups [44,45]. A well-defined narrow peak at 1744 cm^{-1} is relative to the stretching vibrations of C=O from the carbonyl group of esters present in the triglyceride from OP. These are also present in the spectra of the OP composite, confirming its presence. In the same OP spectrum, the band at 1380 cm^{-1} is attributed to the deformation of CH_2 groups. The presence of KL is identified at 1426, 1460, 1520, and 1600 cm^{-1}, due to aromatic skeletal vibrations combined with C–H in-plane deformation, C–H deformations of methyl and methylene, aromatic skeletal vibration breathing with C=O stretching, and C=O stretching (conjugated), respectively. Other typical BNC peaks are present at 1647 cm^{-1} as a result of OH stretching (water absorption) and at 1427 cm^{-1} due to C–H antisymmetric bending. Minor bands at 1410 and 1321 cm^{-1} are due to C–H and O–H antisymmetric bending, at 1315 cm^{-1} due to O–H in-plane bending, at 1203 cm^{-1} due to symmetric stretching vibrations of sulfonic acid groups, at 1161 cm^{-1} from C–O–C asymmetric stretching, and at 1053 cm^{-1} due to C–O stretching. A strong intense peak at 1047 cm^{-1} is from C–O–C stretching vibrations of the ether linkages between pyranose sub-units, at 898 cm^{-1} from the stretching of the C–O–C at ß-(1 → 4)-glycosidic linkages, a small band at 771 cm^{-1} results from bending peaks of CH_2, and at 740 cm^{-1} is due to asymmetric stretching vibrations of sulfonic acid groups [43,44].

2.2.6. Surface chemistry

The XPS survey spectra for BNC and its composites (Fig. S3) display a

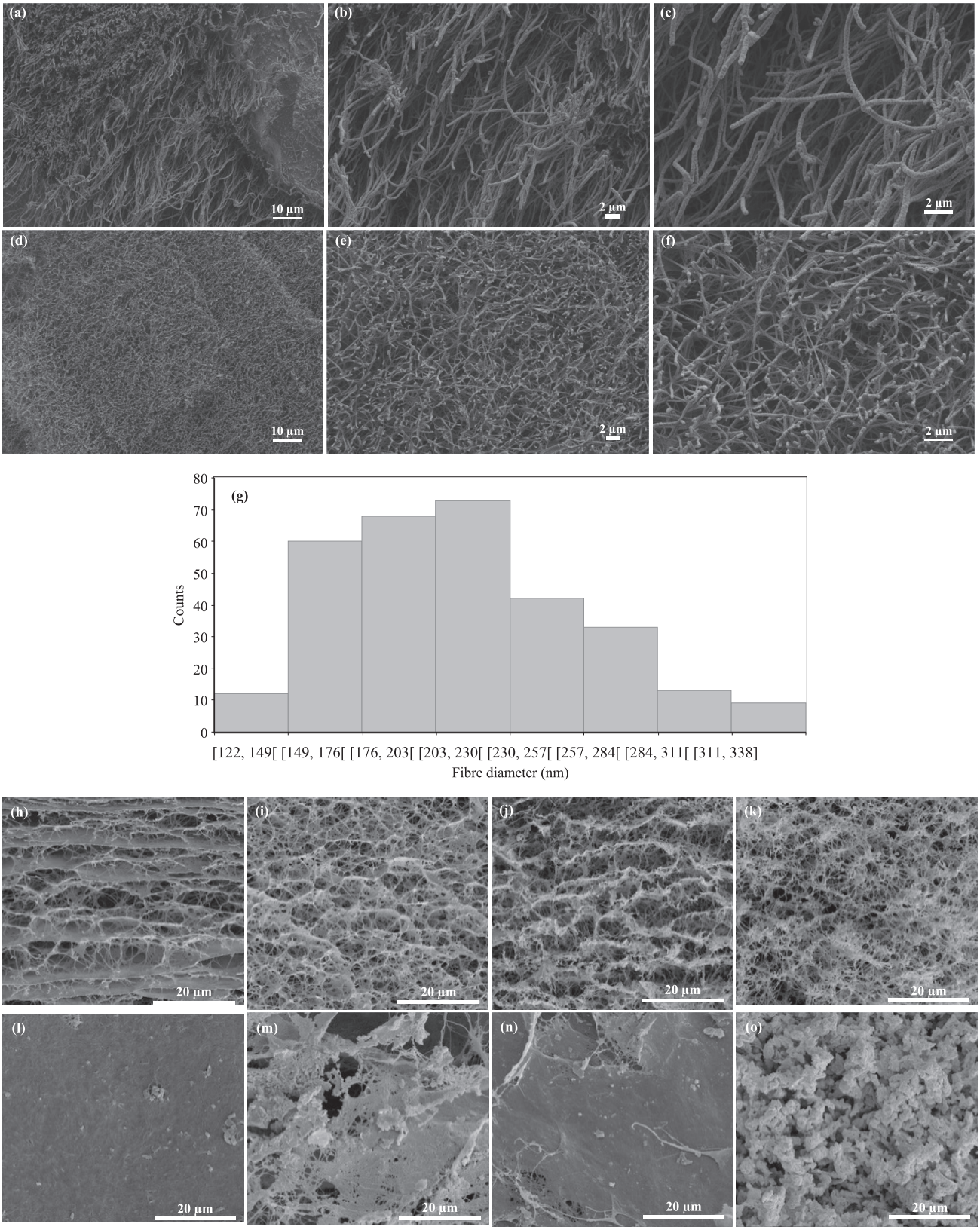


Fig. 4. Cryo-FESEM images of the untreated never-dried samples: cross-section (a–c), and surface (d–f); the histogram related to fibre diameter (o); SEM images of the freeze-dried samples: cross-section of BNC (h), BNC/KL (i); BNC/OP (j), and BNC/KL/OP (k), and surface BNC (l), BNC/KL (m), BNC/OP (n), and BNC/KL/OP (o).

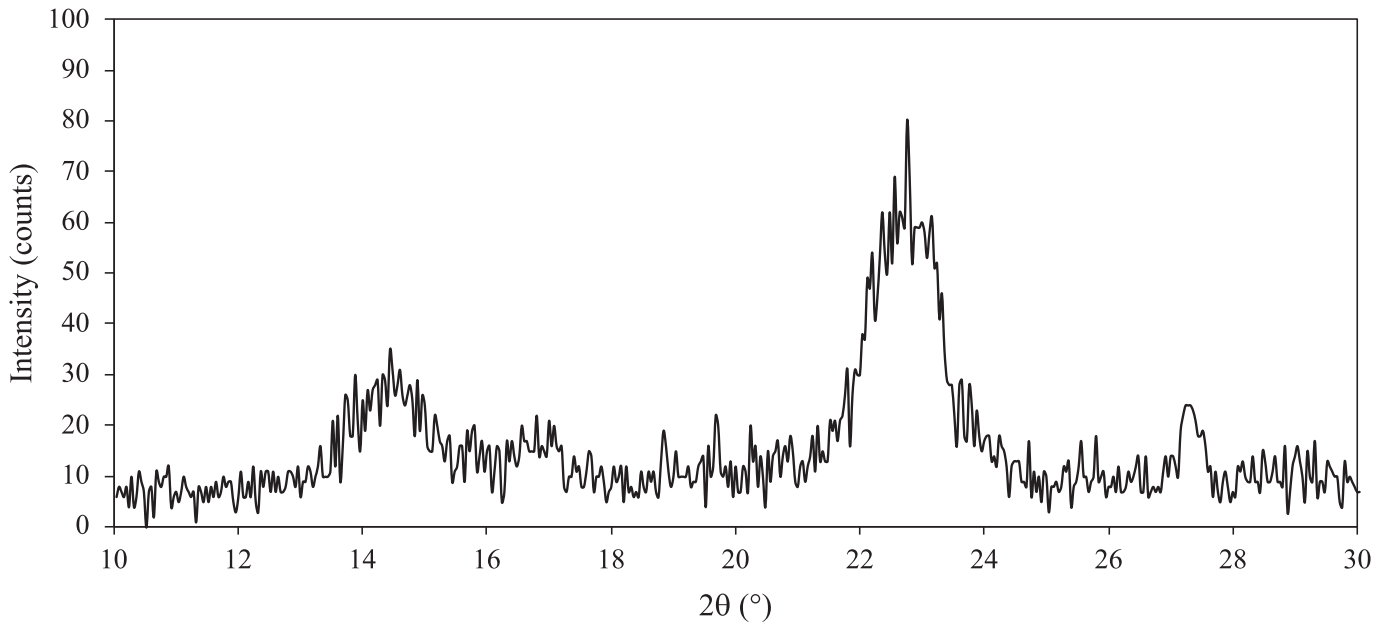


Fig. 5. XDR diffractogram of untreated BNC.

Table 1
Pore size of the BNC composites.

Samples	Pore size (nm)		
	Minimum	Average	Maximum
BNC	135	197	233
BNC/KL	97	129	152
BNC/OP	43	46	48
BNC/KL/OP	87	108	125

considerable presence on the surface of carbon (C1s) and oxygen (O1s) elements. As shown in Table 2, the incorporation of KL and/or OP leads to an increased atomic concentration of the C1s signal, while there is a slight decrease in the O1s concentration. The trend can be explained by the chemical structure of KL and OP, both of which are carbon-based extracts [46,47]. In addition, minor amounts of chlorine (Cl) and nitrogen (N) were detected in the samples, as well as small levels of sodium (Na) and silicon (Si) on the surface. The presence of these elements may be a result of the NaOH-based purification process, which is known to affect the glass of the recipients used [48,49]. Fig. 8a, b presents the C1s and O1s high resolution spectra aligned to the highest C–O–C peak, indicating the highest oxidation in the case of OP modification.

The deconvolution of the C1s spectra is shown in Fig. 8c–f (further details can be found in Table S3). The BNC spectrum presented the three binding energy peaks: 284.7, 286.3 and 287.5 eV, attributed to C–H/C–C, C–O and O–C–O bonds, suggesting an elevated carbon content [50]. The incorporation of KL or/and OP led to an increase in the peak percentage atomic percent (PP At.%) corresponding to C–C/C–H bonds (Fig. 9a). The PP At.% increased from 26.28% in BNC to 27.83, 32.35, and 31.76%, in BNC/KL, BNC/OP, BNC/KL/OP, respectively. This is expected due to the large number of aromatic rings and aliphatic chains present in both KL and OP [21,22]. The peaks referring to C–O bonds, which is the dominant peak for BNC at 286.5 eV, show a decrease in PP At.% after modification OP and KL/OP. Contrarily, these bonds are present in higher percentages in the pristine BNC samples and have also increased with KL. The fact that they decrease could be the result of C–O signal dilution due to the introduction of more hydrocarbons. The peaks at around 288.0–288.5 eV correspond to O–C–O and C=O from acetal, hemiacetal, carboxylic or carbonyl groups [51]. The new peaks at higher binding energies of 289.0, 288.9, and 290.4 eV for KL, OP, and KL/OP composites are related to O=C–O groups of esterified hemicellulose [50]. The combination of KL/OP revealed shake-up satellite peaks due to π→π* transitions in aromatic rings [52]. The π→π* is not expected in pristine BNC samples, thus it could be the result of airborne contamination or even drying [53]. In addition, even after mercerisation, the BNC is unable to completely remove traces of medium and even of cells. Several elements that include double bonds, namely the peptidoglycan with C=O, that is visible in the SEM images, remains entangled in the BNC structure [37].

The increase from 3.55% in pristine BNC to 4.06% in BNC/KL of the π→π* transition indicates that lignin incorporation introduces additional aromatic functionalities. The lower π→π* contribution in BNC/OP (2.80%) suggests weakening or partial alteration of conjugated structures, while the pronounced increase in BNC/KL/OP (6.68%) reflects a synergistic effect between KL and OP, enhancing aromatic conjugation and π electron delocalisation [54]. Furthermore, environmental carbon contamination may contribute to this signal, generating shake-up satellites around 292 eV that mimic π→π* transitions [55]. In addition, partial structural rearrangements during drying or membrane processing may also be responsible. A broadening of the π→π* bond for the BNC/KL/OP composites is the result of the heterogeneous π-systems originating from the mixture [55].

See Fig. 9b presents the O1s binding energy region spectra obtained for BNC and its composites. The BNC possesses its regular peaks, C=O around 531.2 eV, followed by the main peak of BNC, C–O at 532 eV, and by the O–C=O peak around 533.4 eV [56]. The high energy tails between 534–536 eV may be attributed to the presence of water molecules on the surface, in different bonding environments, namely as chemisorbed –OH and physisorbed H_2O. They also appear in BNC to a smaller extent. The contribution of the π −plasmons appears as a shoulder in O1s (typically 536–538 eV), possibly due to O coupling with aromatic π-electrons, which are generated in aromatic materials, from both KL and OP. The fact that the combination of KL and OP induces the strongest tail intensity is due to the synergy among the aromatic structures originating from both compounds. This is in line with the highest intensity of the π–π* bond exhibited in the C1s binding energy region for the same BNC/KL/OP composite material. A similar signal broadening as that encountered in C1s binding energy also appears in this region. The highly energetic tail up to 540 eV suggests that some processes of inelastic losses may appear in the composite material, potentially caused by the sample heterogeneity.

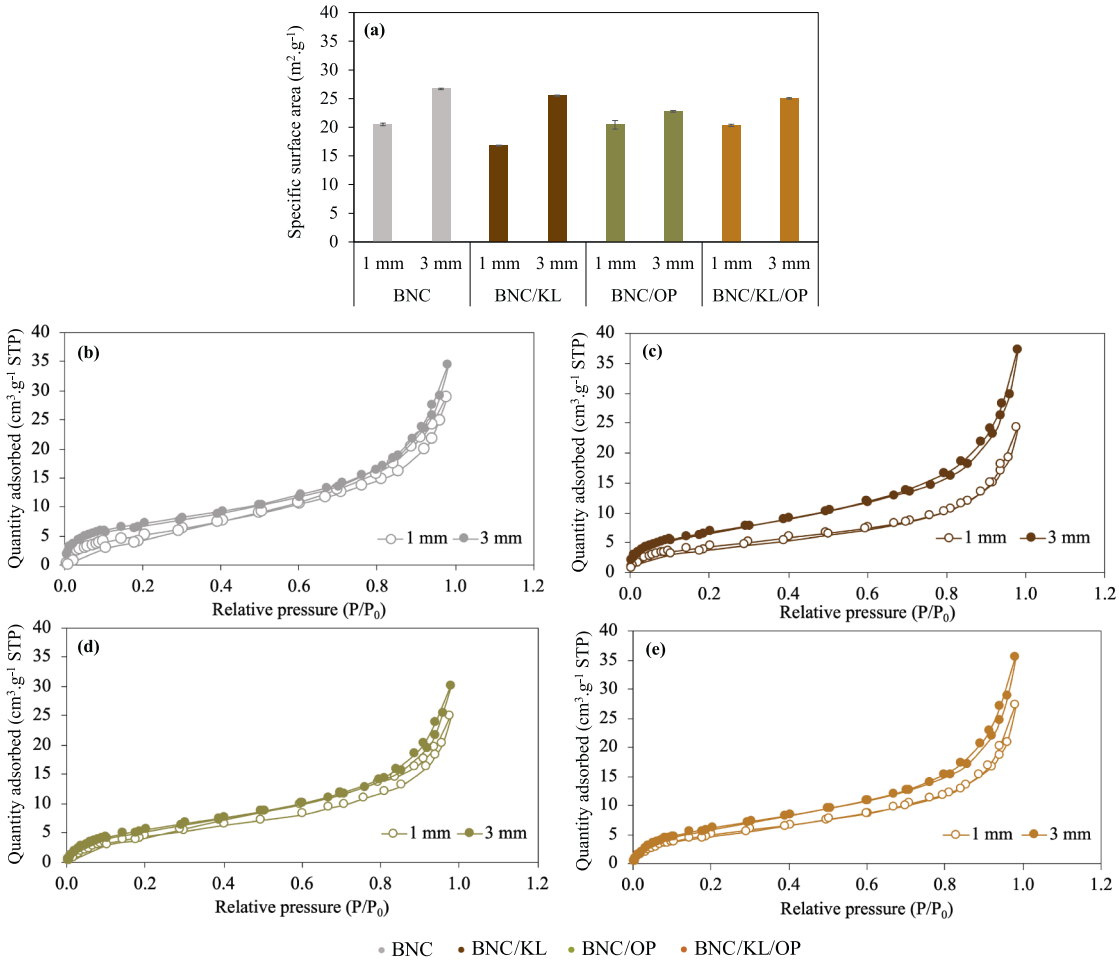


Fig. 6. BET surface area (a), and N_2 absorption/desorption isotherms of BNC (b), and composites BNC/KL (c), BNC/OP (d), and BNC/KL/OP (e).

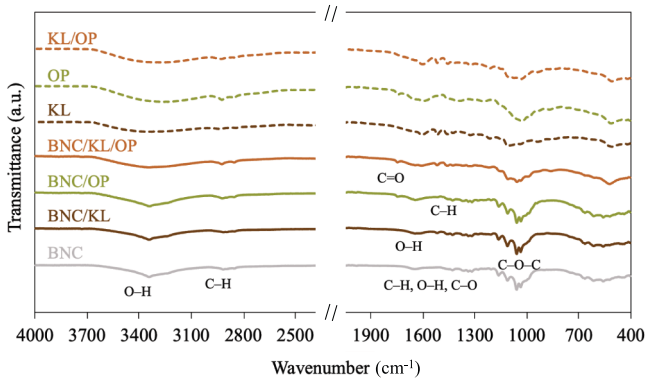


Fig. 7. ATR-FTIR of the extracts and composites developed.

Table 2
Elemental atomic percentages on the surface of the samples from the XPS survey spectra.

Atomic %	O1s	C1s	Cl2p	Na1s	N1s
BNC	33.02	57.66	3.65	2.73	1.7
BNC/KL	31.58	64.05	3.17	–	1.21
BNC/OP	29.81	64.45	4.51	–	1.23
BNC/KL/OP	30.19	63.73	3.69	0.74	1.15

Both XPS and FTIR measurements suggests that the interaction between BNC and KL, OP and KL/OP is predominantly governed by physical adsorption and hydrogen bonding, resulting in a stable surface modification.

2.2.7. *Surface wettability*

The hydrophilicity of an implant surface plays a critical role in the interaction with biological fluids and surrounding tissues due to better protein adsorption. This creates a better environment for cell attachment and differentiation, thus impacting the integration, biocompatibility, and performance of the implant [57,58]. The wettability of the samples' surface was analysed through WCA measurements. Fig. 10 shows that the average WCA are close to or below 20°; therefore, all samples can be classified as hydrophilic (Fig. S4) [59]. These low contact angles may be related to the initial immersion of the samples in the corresponding medium, SBF or aCSF. According to Chen *et al.*, adsorption of BNC (ATCC 53582) in the never-dried state is approximately 50% higher than in the freeze-dried state [60]. The low contact time may be insufficient to achieve complete swelling thus, the majority of the samples did not present statistical differences between the never-dried and freeze-dried physical states. Chemical crosslinking is expected to improve the surface hydrophobicity of the composites [61]. Nonetheless, despite the hydrophobic nature of KL and OP, partially attributed to their aromatic backbone [62], the low WCA values may be the result of the reduced amount of KL (2 wt%) and OP (1 wt%) used in BNC modification [61]. Notwithstanding the hydrophilic nature of these composites, BNC/KL shows statistically significant differences (consult Table S2 for identified outliers) compared to never-dried BNC 1 mm in aCSF and freeze-dried 3 mm for both medium. In contrast, both OP and

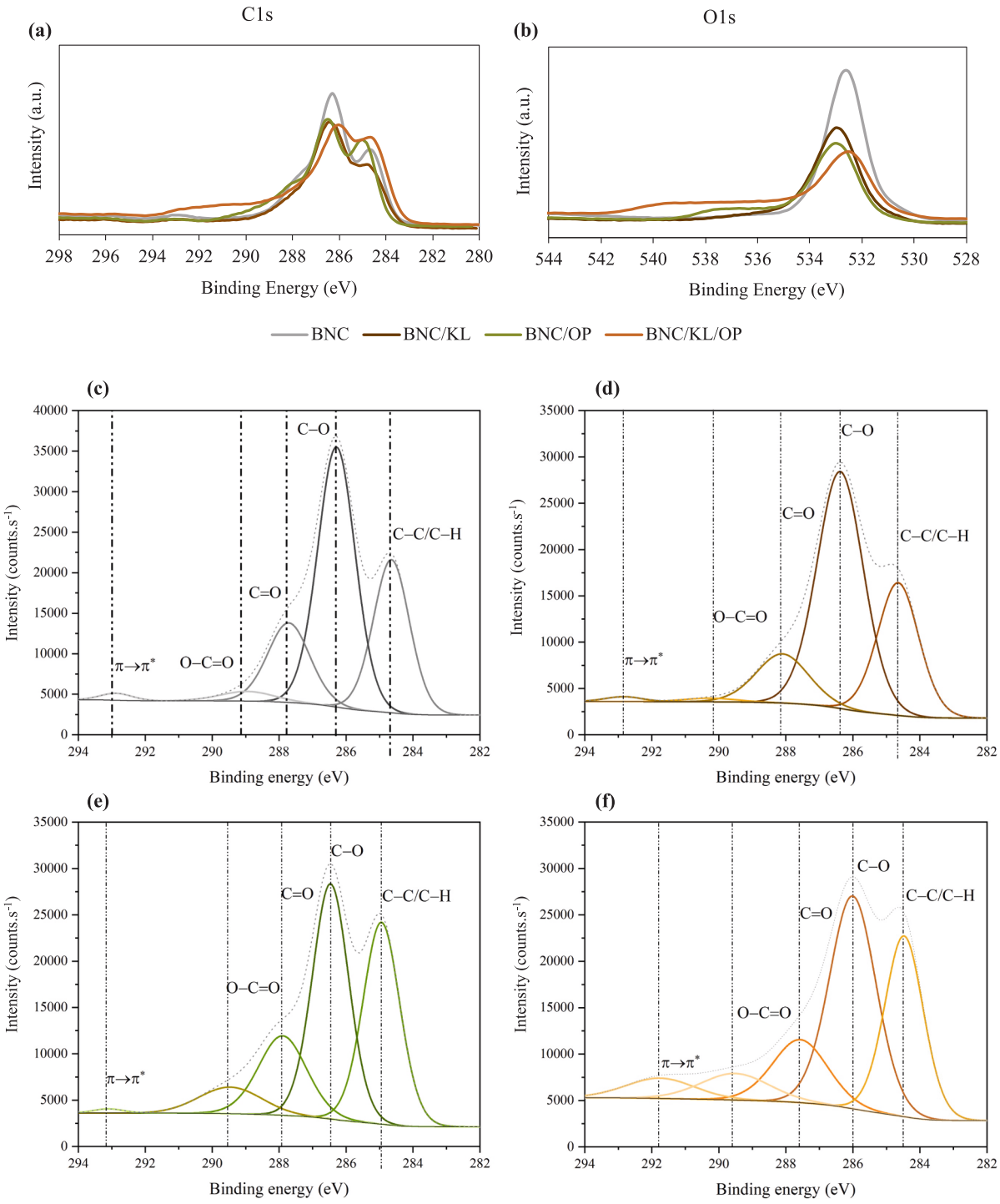


Fig. 8. (a) C1s and (b) O1s spectra of BNC and their composites; and the peak deconvolution at the C1s region obtained for (c) BNC, and composites (d) BNC/KL, (e) BNC/OP, and (f) BNC/KL/OP.

KL/OP composites present statistical differences in relation to BNC in 1 mm freeze-dried BNC composite in aCSF. While statistical differences across samples were verified, all BNC composites present a similar hydrophilic nature.

2.2.8. *Thermal properties*

The thermal analysis of the freeze-dried BNC composites was evaluated through DSC thermograms (Fig. 11a), mass loss curves obtained from thermogravimetrical analysis (TGA) (Fig. 11b), and the differential thermogravimetric (DTG) curves (Fig. 11c). The DSC thermograms of untreated BNC exhibit two characteristic peaks: (Fig. 11a1) moisture release from the samples, either due to physically absorbed molecules or those chemically bound through hydrogen bonds (49–127 °C) (endothermic peak), and (Fig. 11a2) decomposition of cellulose (328–362 °C) (exothermic peak), as confirmed by TGA (Fig. 11b, c). The DSC thermograms of BNC composites reveal two similar peaks, with a third peak corresponding to the decomposition of OP and KL near 200 °C [63]. The degradation profiles of cellulose and lignin are comparable, as evidenced by closely aligned exothermic peaks (344–349 °C), suggesting that KL and OP incorporation did not considerably affect the thermal

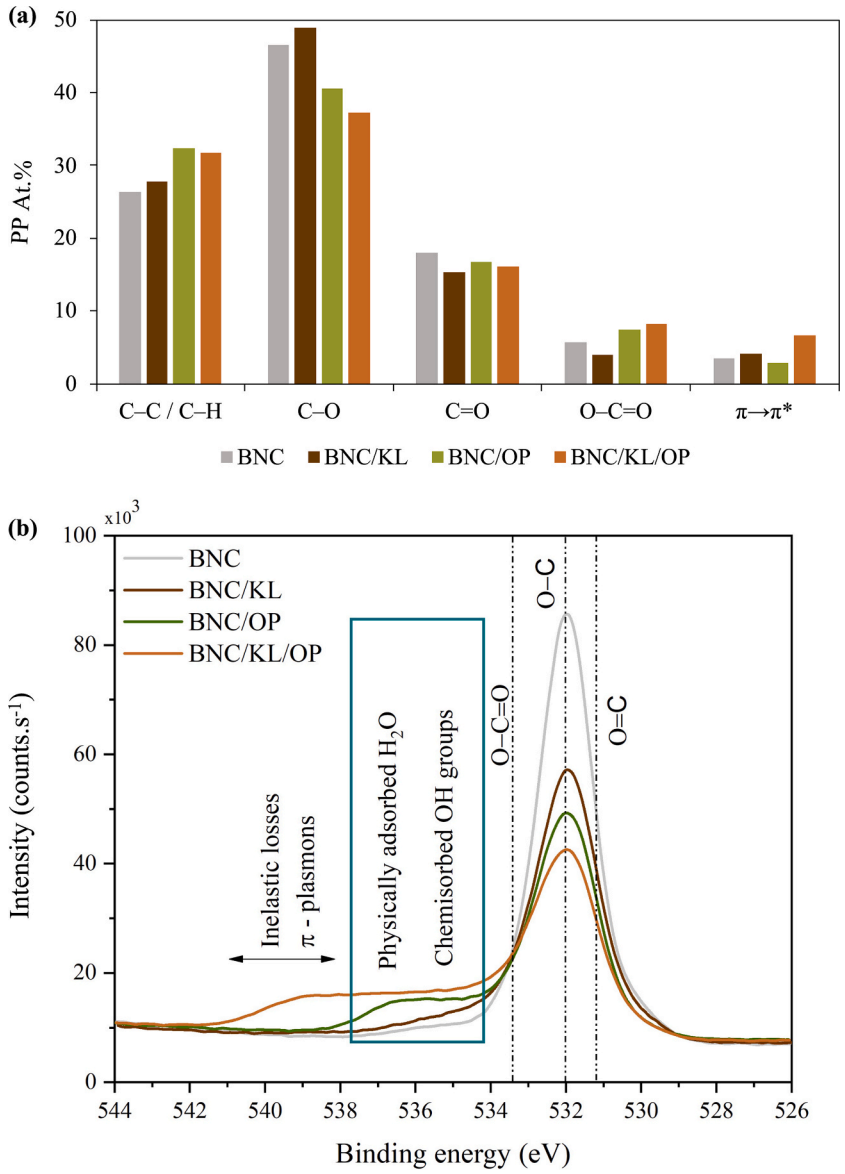


Fig. 9. Carbon bonds contribution for BNC and its KL/OP composites (a), and the O1s binding energy region spectra obtained for BNC and its composites: BNC/KL, BNC/OP, and BNC/KL/OP (b).

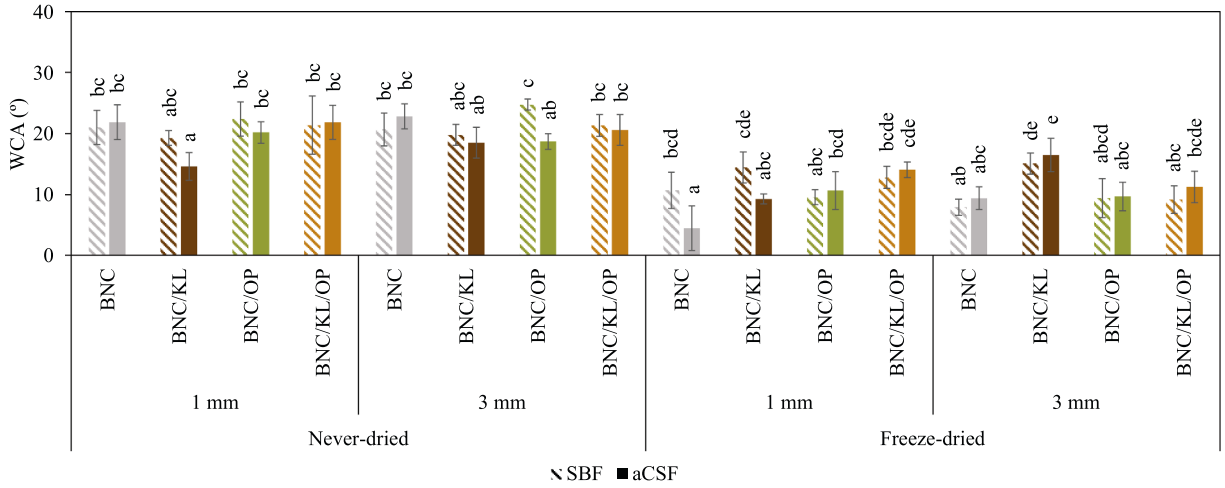


Fig. 10. WCA of the developed composites. Statistical significance was indicated by different letters (a, b, c, d, e) corresponding to a $p < 0.05$.

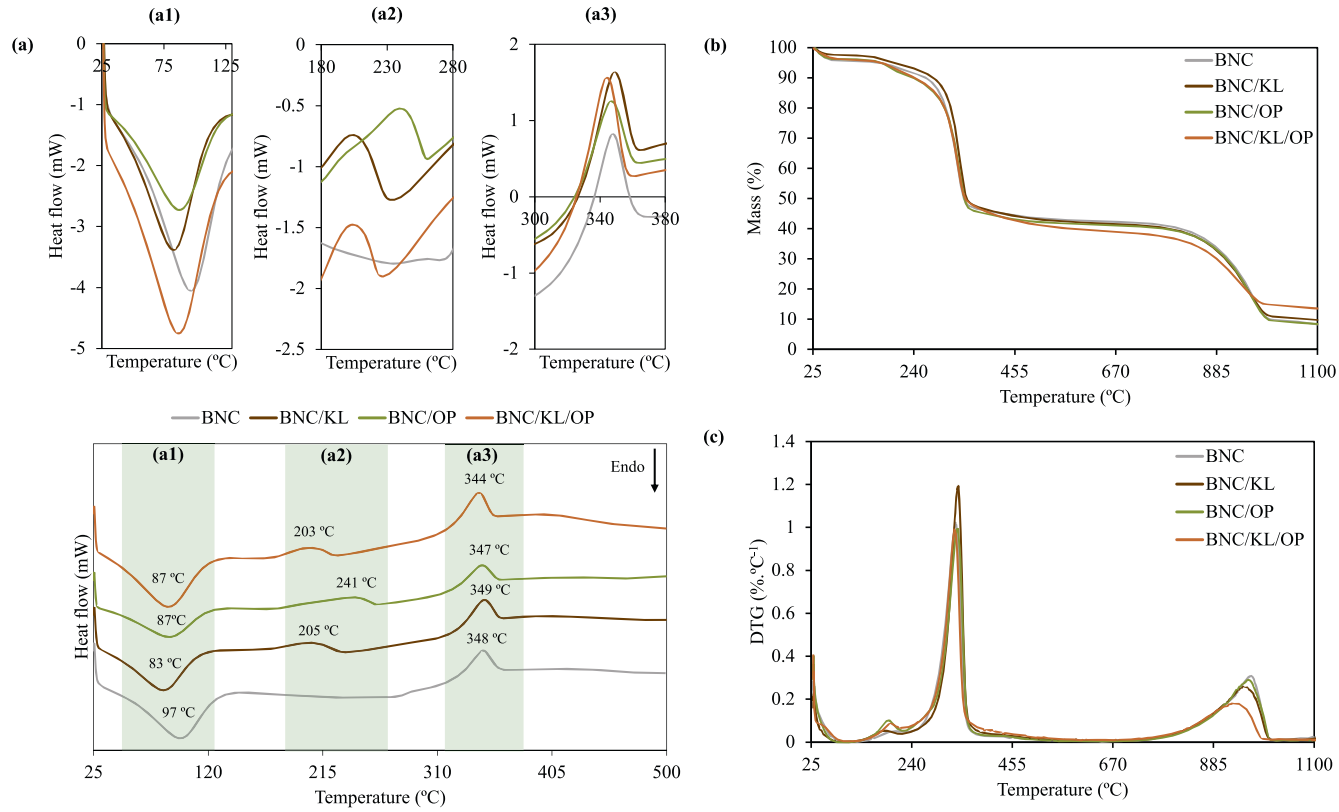


Fig. 11. DSC thermogram (a), TGA curves (b), and DTG curves (c) of BNC composites.

properties of the BNC composites.

The TGA curves show two characteristic processes (Fig. 11b): (i) moisture loss present in the samples or due to hydrogen bonds, and (ii) depolymerisation of β-glucan polymer chains and oxidation of cellulose-based materials into carbonaceous residue [43,64]. Although freeze-dried samples were analysed, residual water was detected due to dehydration and volatilisation within the polymer chain. Nevertheless, the water content remained low, from 4 to 7% between 25 and 105 °C, consistent with the DSC thermogram results [64]. A two-stage decomposition process was observed, with the total mass loss in this process being similar in all composites (~85%), except for BNC/KL/OP, which exhibited a mass loss of 80%. Moreover, a considerably higher mass loss was observed in the second stage of decomposition, considering that the degradation of KL and OP occurs at temperatures of approximately 313–345 °C (Fig. 11c) [65]. The incorporation of KL and OP individually did not affect the thermal properties of the composites, as their decomposition temperatures were similar to that of BNC. This may be attributed to the lack of covalent bonds between these compounds and BNC, and the presence of these biopolymers being limited to the surface of the BNC. The stable aromatic unit characteristic of KL could also contribute to thermal improvements, particularly regarding the maximum degradation temperature (340 °C). Nevertheless, this increase was relatively low, given that the other composites exhibited values ranging from 333 to 338 °C [66]. A higher residual content was obtained in the BNC/KL/OP composite, indicating the presence of a more crystalline structure, which resulted in slightly improved thermal resistance [64].

The results provided by TGA, in combination with FTIR and XRD, show the high purity of the untreated BNC. XRD analysis revealed an exceptional crystallinity index of 94.0%, which was corroborated by FTIR spectroscopy, which showed an effective removal of bacterial proteins and hemicelluloses during the purification process (absence of bands at 1548 and 1730 cm^{-1}), while displaying the dominant C–O–C stretching vibrations at 1033 cm^{-1} [67]. Furthermore, TGA confirmed the high thermal stability of untreated BNC, exhibiting a degradation temperature of 348 °C, characteristic of crystalline cellulose I. Overall, these results demonstrate the purity of untreated BNC.

2.2.9. *Swelling ratio determination*

The swelling behaviour of BNC composites is partially related to their hydrophilic properties and drug release in response to a biological fluid, and it influences the biocompatibility of the implant [58]. The swelling ratio of never-dried and freeze-dried BNC composites was evaluated by measuring the swelling ratio in SBF and aCSF solvents (Fig. S1). Fig. 12 illustrates the equilibrium swelling values observed for each condition, while Fig. S5–S8 present the complete swelling curves.

Freeze-dried samples exhibit statistically higher swelling compared to never-dried membranes. The increased swelling in freeze-dried samples (Fig. 12a) can be attributed to their hydrophilic nature, higher porosity (as displayed in Fig. 4h–o and Table 1), a higher pore number, which collectively enhance the diffusion of biological fluid (SBF and aCSF) and the swelling rate [36]. In addition, the pore size may have increased due to ice crystal formation during the freeze-drying process, thereby facilitating fluid permeation and diffusion [68]. Freeze-dried samples with a thickness of 3 mm generally exhibit higher swelling capability than those with a thickness of 1 mm, suggesting that thickness directly influences porosity and water absorption [69,70]. Composites in the never-dried and freeze-dried states showed statistical differences for 1 mm thick BNC in SBF, whilst in aCSF BNC, BNC/KL, and BNC/KL/OP differ (Fig. 12). Despite the similar ionic character of SBF and aCSF with nearly identical pH (7.2 for aCSF and 7.4 for SBF, Table S1), these media differ in salt composition and respective concentration. Furthermore, the lower concentration of H^+ ions minimises electrostatic repulsion, thereby facilitating adsorption or hydrogen bonding with water molecules [36,71,72]. In never-dried composites, no statistical difference between the release media aCSF and SBF. However, statistical differences were observed for the different thicknesses in SBF for BNC and BNC/KL/OP, and only for BNC/KL/OP in aCSF (Fig. 12b). The

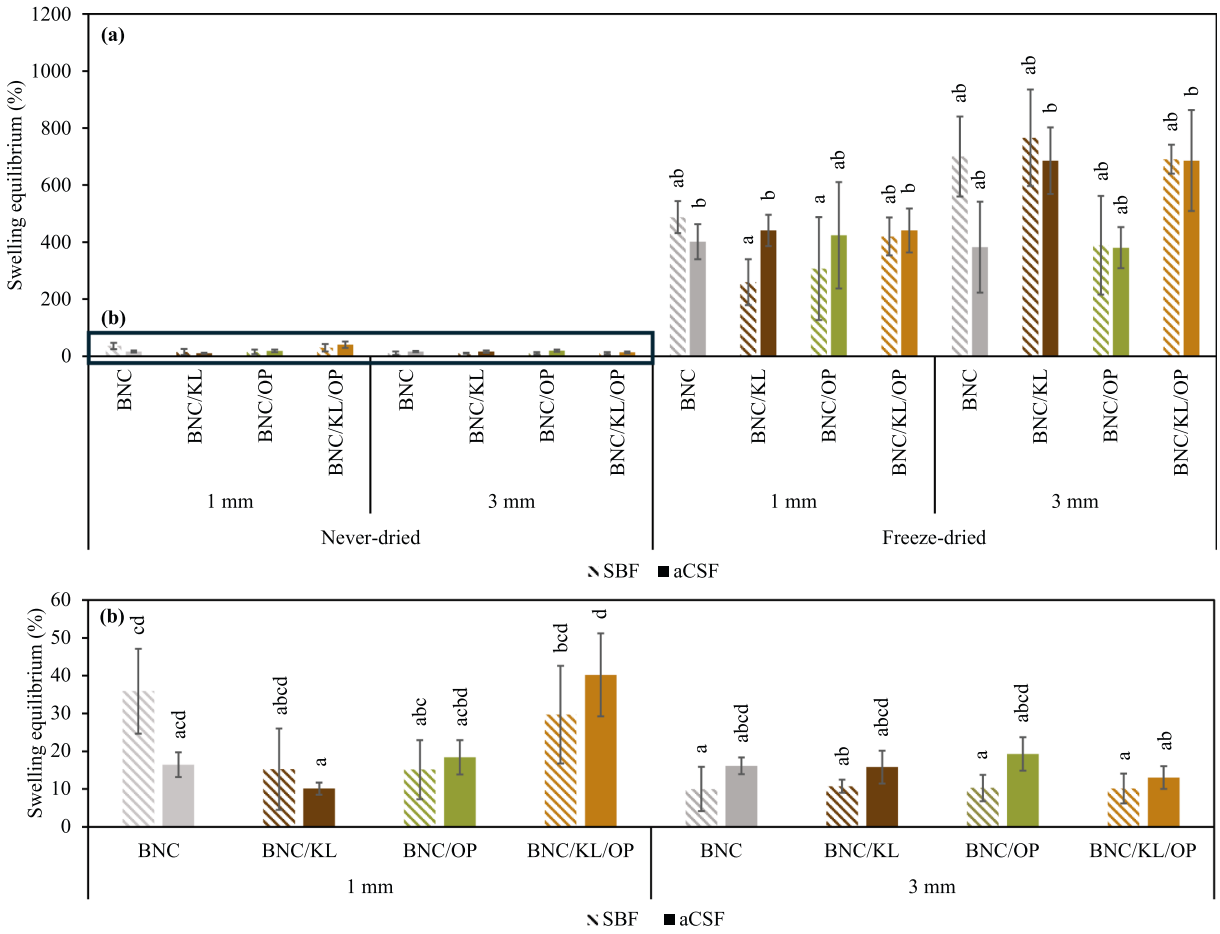


Fig. 12. Swelling of BNC composites (a) and never-dried composites (b), pristine and modified composites, with thicknesses of 1 and 3 mm, using SBF and aCSF as solvent. Statistical significance was highlighted by different letters (a, b, c, d) when $p < 0.05$.

swelling difference between the modified samples can be attributed to the limited crosslinking between BNC and KL or OP, as well as the inability of these macromolecules to penetrate the porous structure of BNC. The hydrophobic properties of KL and OP should result in reduced swelling. However, the pore size measurements, presented in Table 1, showed the influence of OP particles in the reduction of the composite's pore size.

2.2.10. *In vitro release of KL and OP*

The release profile of KL, OP, and KL/OP is shown in Fig. 13. For 1 mm thickness BNC, the release is sustained over time, and the highest release percentage is only slightly above 0.1%. This minimal percentage may be due to the large size of the organic particles being unable to enter the nanofibrous structure, due to the smaller pore size of the BNC, as confirmed in Fig. 4g–j, 6a. Moreover, despite the hydrophilicity and elevated swelling of BNC (as confirmed in Figs. 10 and 12), which could suggest high release rates, the hydrophobic nature of the extracts and their electrostatic interaction with BNC decreases their diffusion into the aqueous media [62]. This low and constant release is also verified for the 3 mm thickness BNC, which reaches a maximum of 0.3%, as demonstrated in Fig. 13. For OP and KL/OP 3 mm thickness samples, specifically, the release rates are slightly higher in the initial hours until approximately 100 h, after which a gradual decrease is observed. Nevertheless, considering the percentages, this could be regarded as minimal. The controlled release of the samples is beneficial since it improves patient compliance and reduces side effects, particularly toxic effects [73]. In line with the sample thickness, the medium in which the samples were immersed affects the release rate, being higher for those immersed in SBF compared to aCSF. On the contrary, the physical state of the BNC composites does not have an influence on the release rate.

The fitted experimental data are presented in Table S4–S7 and Fig. S9–S12, and include Korsmeyer-Peppas, Makoid-Banakar, Weibull, Logistic, Gompertz, and Probit models, which apply a nonlinear least-squares curve-fitting technique [74,75]. The drug release models' fitting quality was evaluated using the coefficient of determination (R^2) values and the Akaike Information Criterion (AIC), for which there is no absolute value. Instead, a comparison between the lowest AIC value indicates the better-fitting model [76]. The R^2 and AIC values can be consulted in Table S4–S7. The release mechanism is primarily governed by burst surface desorption rather than matrix diffusion. This is evidenced by the Korsmeyer-Peppas n values being considerably below 0.45 (ranging from −0.029 to 0.099), which characterizes a quasi-instantaneous release profile or burst effect. The relatively poor fit of the standard diffusion models ($R^2 < 0.814$) further supports the conclusion that the KL/OP molecules are physically adsorbed to the BNC surface, consistent with the XPS and FTIR findings of non-covalent interactions. The mathematical modelling results show that no model was able to adequately predict the release data obtained, due to the very low release percentages.

2.2.11. *Antimicrobial properties of the extracts*

The direct determination of the MIC of each extract through the checkerboard assay (Fig. S2) is only considered for growth percentages lower than or equal to 20% [77]. OP was effective at 1.25 $g.L^{-1}$ against most microorganisms, except for *C. albicans* (2.5 $g.L^{-1}$, the maximum tested concentration) and the propagation of MS2 bacteriophage (0.08 $g.L^{-1}$). Sunthornvarabhas and co-workers reported a MIC of 4.096 $g.L^{-1}$ against *S. aureus* for lignin extracts of sugarcane bagasse [78]. The

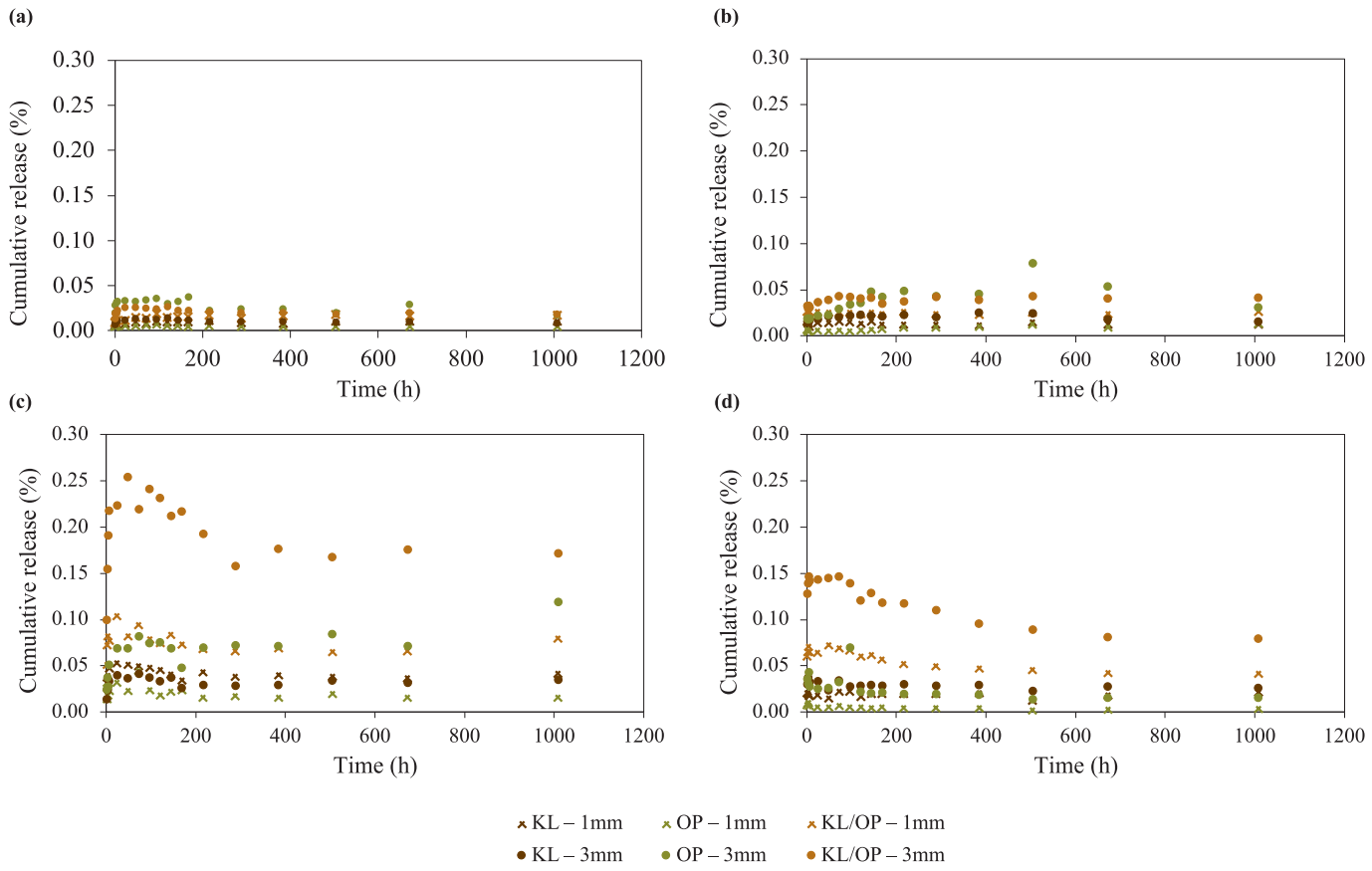


Fig. 13. Cumulative drug release profiles of KL, OP, and KL/OP throughout 1008 h for never-dried (a) and freeze-dried (b) composites in aCSF, and for never-dried (c), and freeze-dried (d) composites in SBF.

obtained MIC values for KL varied, with the lowest of 0.05 $g.L^{-1}$ obtained against *C. krusei*, and the highest, 25.60 $g.L^{-1}$, against *P. aeruginosa*. Dong *et al.* reported MIC values for KL of 2.5 $g.L^{-1}$ against *S. aureus*, higher than the 0.40 $g.L^{-1}$ achieved in this work [79]. Despite Reyes *et al.* reporting no activity of KL against *S. aureus*, the results showed activity at a concentration of 0.40 $g.L^{-1}$ [22].

These MIC values are used to calculate FICI, and from these, the synergy of both extracts can be determined. Despite the high MIC values of the individual compounds, according to Fig. 14, synergy was obtained within the larger variation of KL/OP concentrations against *P. aeruginosa*. Both *S. aureus* and *C. albicans* were also sensitive to the mixture at lower concentrations of KL and OP. Nevertheless, a synergetic effect was not observed against *C. krusei* nor MS2. Some additive or indifferent effects are also shown in Fig. 14. The antagonistic effect observed for most of the tested microbes, particularly the bacteriophage, can be explained by the agglomeration of both extracts, especially considering that this negative effect occurs mainly at higher concentrations of both extracts. This effect is less extended against *P. aeruginosa*.

2.2.12. Antimicrobial properties of the composites

KL and OP antimicrobial activity has been thoroughly described and is attributed to the phenolic fragments holding a double bond in the Cα = Cβ position of the side chain and a methyl group in the γ position. These phenolic groups lead to bacteria's death when in contact with the cell membrane, prompting bacterial lysis [80,81]. Kraft lignin presents antibacterial effect through disrupting bacterial membranes, promoting cell lysis, and inducing reactive oxygen species, which cause oxidative stress, such as lipid and DNA damage, and inhibit bacterial growth [23]. The assessment of the antimicrobial activity of the BNC composites was performed using the shake flask and the contact killing assays. According to Fig. 15, no antimicrobial activity was observed using the shake flask methodology. This method is strongly dependent on the release of the bioactive compound. Despite the verified statistical differences, the statistical analysis was not discussed, considering the lack of activity (all results show log reduction lower than 1). These findings are in agreement with the controlled release data (Fig. 13) that show a negligible release of the extracts from the BNC substrates, likely due to the hydrophobic nature of KL and OP [62].

The contact killing results in Fig. 16 showed no antibacterial nor antifungal activity for never-dried 1 mm thickness samples. The 3 mm thickness samples showed activity against bacteria or yeast, with the KL (*S. aureus*), OP (*P. aeruginosa*) and KL/OP (*S. aureus* and *P. aeruginosa*) composites obtained log reductions of approximately 2. No statistical differences were determined for all samples between the different thicknesses against *P. aeruginosa* and *S. aureus*, except for never-dried BNC/KL and BNC/KL/OP (*S. aureus*). Regarding the antiviral activity, the MS2 bacteriophage seems to be vulnerable to BNC/OP (1 and 3 mm) and to BNC/KL/OP composites (3 mm thickness), with log reductions of 4. Statistical differences were found between thicknesses only in never-dried BNC/KL/OP. In the case of 1 mm thickness samples, the control obtained a 2 log reduction, which, despite being high for a control sample, does not invalidate the 4 log reduction for BNC/OP and BNC/KL/OP composites. The reason could be hypothetically attributed to the high electrostatic forces established between BNC and the virus. This is based on the results obtained with cotton knitted structures, where 1 log reduction was observed for control samples. In this case, the effect is enhanced due to the high surface area provided by the nanostructured BNC [82].

For freeze-dried BNC composites, antimicrobial activity was verified for OP and KL/OP 3 mm composites against *S. aureus* (2.5 and 2.6 log reduction). No statistical differences were observed for all composites.

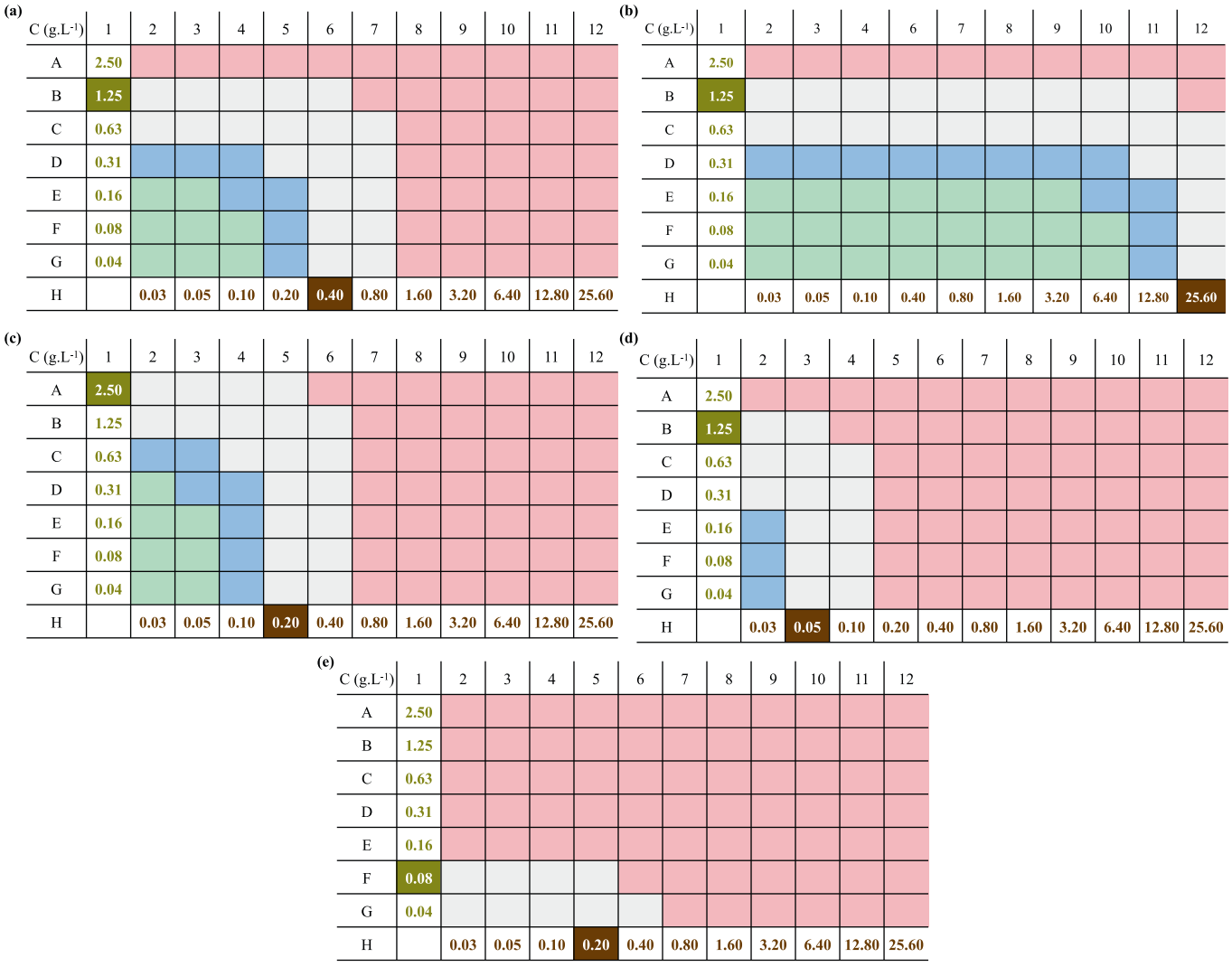


Fig. 14. MICs (g.L^{-1}) of KL (■) and OP (■) used for fractional inhibitory concentration index (FICI) calculations and the (■) synergistic, (■) additive, (■) indifferent or (■) antagonist effect of the mixtures for *S. aureus* (a), *P. aeruginosa* (b), *C. albicans* (c), *C. krusei* (d), and MS2 bacteriophage (e).

The 4 log reduction obtained against *P. aeruginosa* for the control suggests that this particular strain may be more prone to dehydration, even with the 30 min contact time reduction. In fact, activity against Gram-negative bacteria is unexpected due to the double peptidoglycan layer, whilst Gram-positive *S. aureus* possesses a single layer, making *P. aeruginosa a priori* less susceptible to antimicrobial agents [83]. This is supported by the MIC values obtained for KL against *P. aeruginosa*, which was the highest concentration tested, 25.60 g.L^{-1}. Nevertheless, the best results obtained against *P. aeruginosa* are corroborated by the checkerboard assay, with the most synergetic effect compared to the other tested microorganisms. Other factors that could influence the antimicrobial activity are the surface charges of the bioactive agents. Gram negative bacteria have a higher negative surface charge, which could also explain the unexpected effectiveness against *P. aeruginosa*. The antimicrobial activity against Gram-positive bacteria can be justified by a higher electrostatic interaction and hydrogen bonding between the cell membrane and the KL moieties [83]. Despite the low antimicrobial activity obtained, liquor pulp precipitated lignins, as is the case with KL, are reported to be efficient against Gram-positive bacteria, like *S. aureus*, but not towards Gram-negative bacteria, as is the case with *P. aeruginosa*. In general, the reduced antibacterial efficiency of KL towards Gram-positive bacteria is due to the aliphatic –OH groups from the carbohydrates [80]. In addition, the difference in the antimicrobial activity of the different lignins may also be attributed to the extraction and preparation methods, pH and temperature [80]. Yang *et al.* reported antibacterial activity of lignin nanoparticles/polylactic acid against both Gram-positive and Gram-negative bacteria, suggesting that another influencing factor could be the size [84]. The stability of OP was discussed by Lammi *et al.*, who suggest that the OP grinding and drying process at 60 °C for 24 h may cause denaturation of the bioactive compounds [85]. Furthermore, other authors suggest that the thawing process, or even the period during which the OP remains at room temperature, may affect its properties. Hydrolysis of secoiridoids affects the concentration of the main phenols, thus altering the phenol constituents, which in turn affects the antibacterial activity [86,87]. Antiviral activity was found for 3 mm thickness BNC/KL/OP composites with 2.4 log reduction, being statistically different from the remaining never-dried samples of the different thicknesses. The 2 log obtained for 1 mm samples cannot be validated due to having the same values as the control sample.

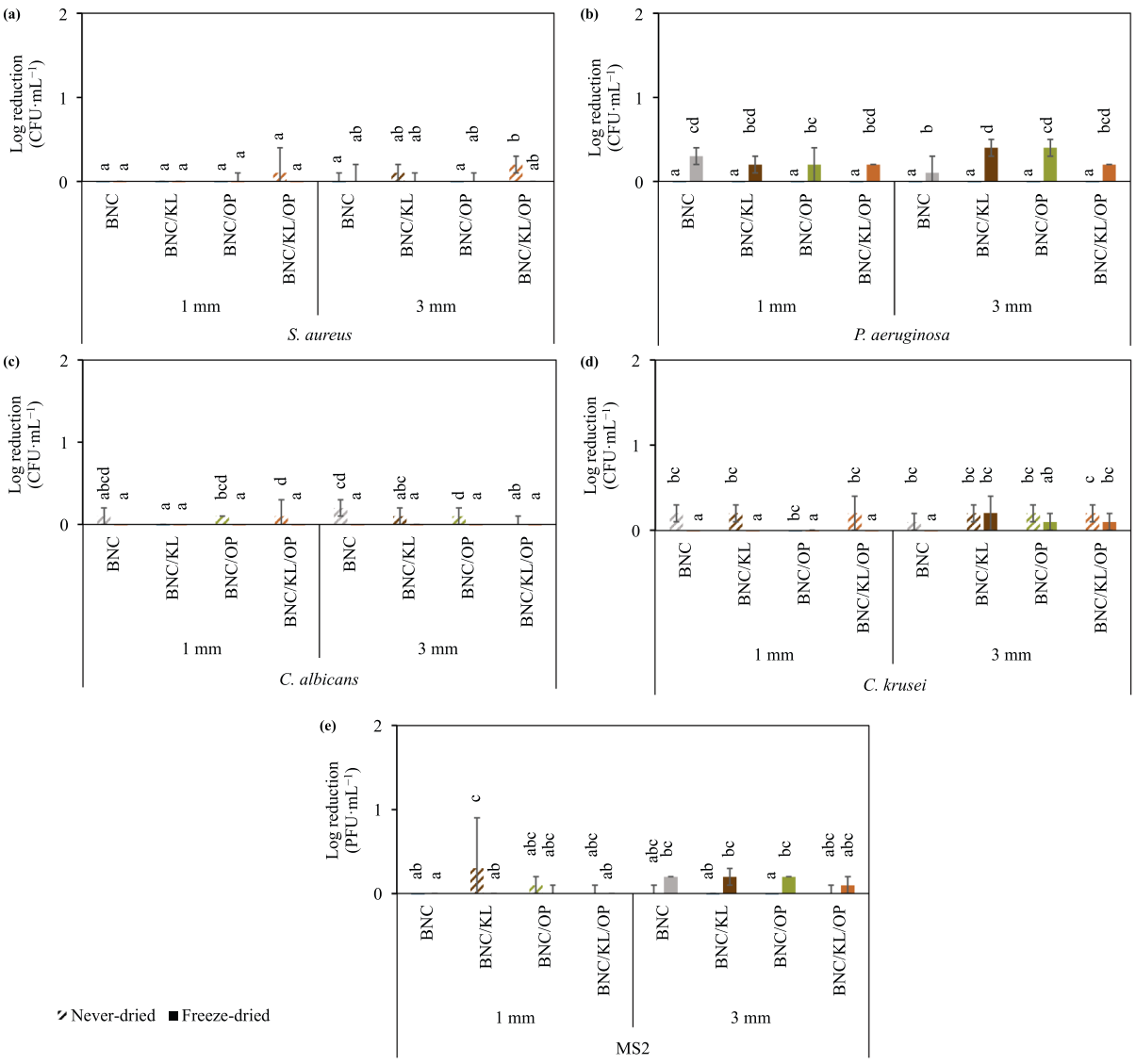


Fig. 15. Shake flask of BNC nanocomposites with 1 and 3 mm thicknesses for never-dried and freeze-dried samples against *S. aureus* (a), *P. aeruginosa* (b), *C. albicans* (c), *C. krusei* (d), and MS2 (e). Statistical significances were indicated by different letters (a, b, c, d) when $p < 0.05$, however, these differences were disregarded due to the lack of antimicrobial activity.

Usually, a log reduction between 2 and 3 is required to be considered antimicrobial, it may also depend on the type of application [88]. Thus, according to the present results, no significant antimicrobial activity is verified. This may be due to the low release and size of the extracts. Although several authors in the literature state that KL has antimicrobial activity, it should be considered that this property is variable, since it depends on the source and extraction method. Furthermore, OP has shown bacteriostatic effect against different pathogens [89].

2.2.13. *Antioxidant properties*

The implantation of biomaterials (bioimplant) into the human body induces an inflammatory response, primarily motivated by oxidative stress resulting from increased reactive oxygen species (ROS) production [90]. Therefore, implants should exhibit antioxidant activity to neutralise ROS and prevent the establishment of an oxidative environment that could compromise their long-term stability. KL and OP possess methoxy and phenol groups in their structure, contributing to their antioxidant activity and reducing the ROS concentration [91–93]. Thus, the antioxidant activity of BNC composites (never-dried and freeze-dried) was evaluated using the DPPH assay (Fig. 17).

BNC does not exhibit intrinsic biological properties; however, a residual antioxidant activity (below 20%) was observed, as reported in the literature [94,95]. Following the incorporation of polyphenol agents, this biological property generally increased. Phenolic compounds produce ROS that can either contribute to antibacterial and antioxidant activity, or potentially damage cells. However, animal cells are less prone to oxidative damage than bacteria, due to the cell's ability to mitigate cytotoxic effect [23]. In addition, the release of macromolecules over time was found to be residual, suggesting that they are unlikely to induce cytotoxic effects or compromise cell viability. KL reaches an initial boost compared to OP, which could, on one hand, be attributed to the larger particle size of KL that is more available at the BNC surface. On the other hand, and according to Table 1, BNC/OP presents a lower pore size, which indicates the presence of smaller OP particles inside the pores and greater phenolic content, both of which are believed to enhance diffusion efficiency [96]. DPPH is a small molecule (nearly 1 nm), thus it is able to permeate through the pores of BNC interacting with KL and OP inside the BNC, despite the low release profile verified. Therefore, the antioxidant activity of BNC/OP increases over time, reaching a higher percentage at 24 h compared to BNC/KL (statistical

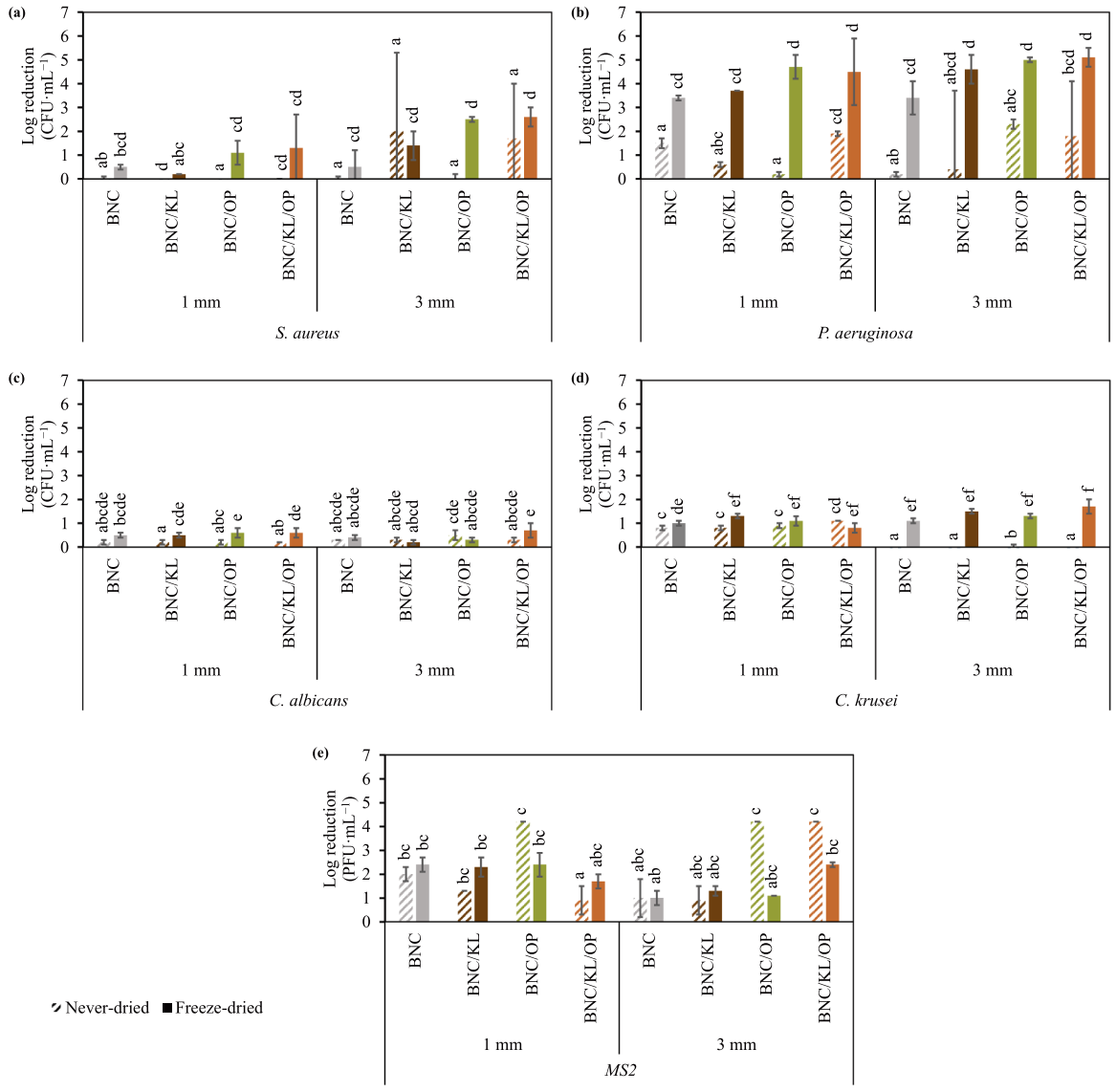


Fig. 16. Contact killing of BNC nanocomposites with 1 and 3 mm thicknesses for never-dried and freeze-dried samples, against *S. aureus* (a), *P. aeruginosa* (b), *C. albicans* (c), *C. krusei* (d), and MS2 (e). Statistical significance was indicated by different letters (a, b, c, d, e, f) when $p < 0.05$.

difference, $p < 0.05$). This may be justified by the lower diffusion of OP particles that required a longer period. Crugeira *et al.* demonstrated that BNC produced using OP hydrolysate as a substrate exhibited a more gradual release of phenolic compounds, which corresponded to an increased antioxidant activity of approximately 40% in DPPH assays [48]. However, the antioxidant activity of BNC/KL/OP diminishes after 24 h (no statistical difference, $p < 0.05$). In contrast, in the present study, a maximum activity of around 80% was achieved in the freeze-dried samples. The BNC/KL/OP composites showed activity compared to never-dried composites, likely due to their larger particle size and lower porosity, which may limit the effective release of active compounds. This antioxidant activity may help neutralise the ROS generated during inflammatory processes, which is particularly important for implants given the high incidence of post-operative complications.

3. Conclusions

The development of biobased medical implants is mainly warranted for their potential to mitigate foreign body reaction, lower the potential of local and systemic cytotoxicity. The extension of their longevity is also a relevant property, as it is directly correlated with a potential reduced recurrence. Furthermore, the propensity for providing bioactivity, using biomolecules, falls within the same advantages. In this exploratory study, the use of BNC as a nanofibrous matrix for the incorporation of the KL, OP, and KL/OP microparticles as bioactive agents may be an option for the development of new implantable materials, in particular due to their reasonable cost and ability to withstand the autoclave. The modification process was performed via exhaustion, a nearly ubiquitous method in textile processing. Two BNC states: never-dried and freeze-dried, and two thickness values (1 and 3 mm) were assessed. The presence of KL, OL, and KL/OP in the BNC was clearly observed, with considerable impact on the pore size of the BNC. However, no clear differences in the specific surface area were detected. The hydrophilic nature of the composites positively promotes the adhesion of host cells and proteins. Nevertheless, it may also promote bacterial, fungal, and viral adhesion. Thus, antimicrobial activity is a key feature of medical implants. The antimicrobial activity ranged between weak decontaminant and moderate disinfectant, proving to be effective in direct contact against *S. aureus*, *P. aeruginosa*, *K. krusei*, and MS2. The antimicrobial activity was overall higher for the freeze-dried samples. However, no activity was observed against *C. albicans*. The antimicrobial activity was associated with moderate to high antioxidant activity, with

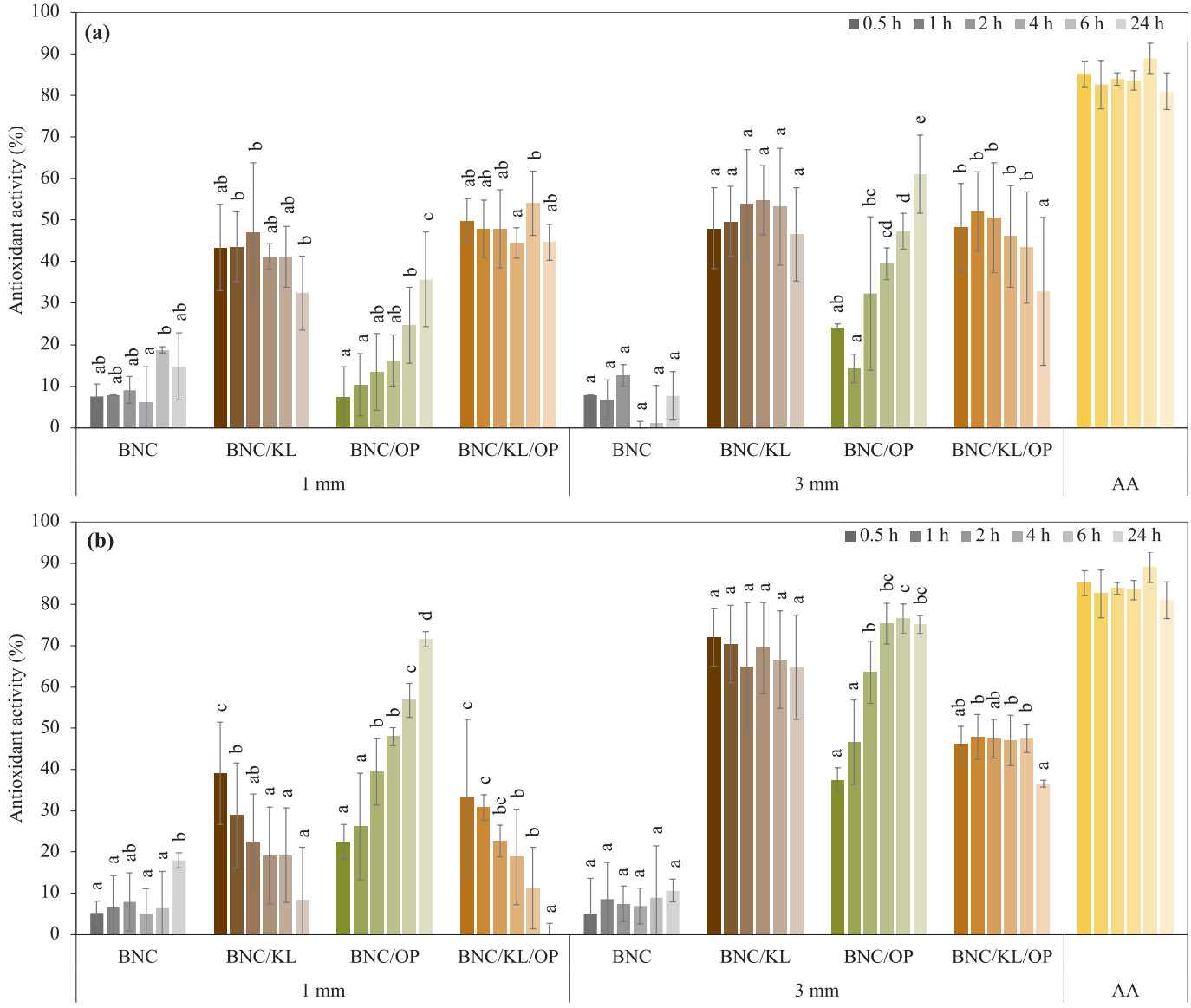


Fig. 17. Antioxidant activity of BNC composites: never-dried (a) and freeze-dried (b). Statistical significance was indicated by letters (a, b, c, d) when $p < 0.05$. AA was used solely as positive control.

the freeze-dried samples exhibiting the highest activity. Interestingly, the same trend of activity per bioagent is consistently maintained. Thus, the improvement observed in the freeze-dried samples may be due to the significantly higher swelling observed, which most likely facilitated the interaction with DPPH. A highly important feature of all composites was the marginal release of the bioactive molecules (between nearly 0.01 and 0.25% up to 1,000 h). This minor release was independent of the swelling of the freeze-dried samples which exceeded 200%. The absence of leaching of the bioagents encompasses critical advantages: it diminishes the loss of activity by dilution, improves longevity, and may mitigate potential systemic cytotoxicity.

CRediT authorship contribution statement

Liliana Melro: Writing – review & editing, Writing – original draft, Visualization, Validation, Methodology, Investigation, Formal analysis, Data curation, Conceptualization. **Cátia Alves:** Writing – review & editing, Writing – original draft, Visualization, Validation, Methodology, Investigation, Formal analysis, Data curation, Conceptualization. **Marta Fernandes:** Writing – review & editing, Visualization, Validation, Methodology, Investigation, Data curation, Conceptualization. **Rui D.V. Fernandes:** Writing – review & editing, Visualization, Validation, Investigation, Conceptualization. **Adriana Pereira:** Writing – review & editing, Visualization, Validation, Investigation. **Diego Moldes:** Writing – review & editing, Visualization, Validation, Resources, Investigation, Funding acquisition. **Ana Cristina Rodrigues:** . **Vitor Sencadas:** Writing – review & editing, Validation, Resources, Investigation. **Bogdana Mitu:** Writing – review & editing, Validation, Resources, Investigation, Formal analysis, Data curation. **Veronica Satulu:** Writing – review & editing, Validation, Resources, Investigation, Formal analysis, Data curation. **José Lourenço:** Writing – review & editing, Validation, Resources, Investigation, Formal analysis, Data curation. **Giorgio Pace:** Writing – review & editing, Validation, Resources, Investigation, Formal analysis, Data curation. **Luis A. Martins:** Writing – review & editing, Validation, Resources, Investigation. **José Luis Gómez Ribelles:** Writing – review & editing, Validation, Resources, Investigation. **António J. Salgado:** Writing – review & editing, Validation, Supervision, Investigation. **Jorge Padrão:** Writing – review & editing, Writing – original draft, Visualization, Validation, Supervision, Project administration, Methodology, Investigation, Formal

analysis, Data curation, Conceptualization. **Andrea Zille:** Writing – review & editing, Writing – original draft, Visualization, Validation, Supervision, Resources, Project administration, Methodology, Investigation, Funding acquisition, Formal analysis, Data curation, Conceptualization.

Declaration of competing interest

The authors declare that they have no known competing financial interests or personal relationships that could have appeared to influence the work reported in this paper.

Appendix A. Supplementary data

Supplementary data to this article can be found online at https://doi.org/10.1016/j.compositesa.2026.109970.

Data availability

Data will be made available on request.

References

[1] Liu G, He Y, Liu P, Chen Z, Chen X, Wan L, et al. Development of Bioimplants with 2D, 3D, and 4D Additive Manufacturing Materials. Engineering 2020;6(11):1232–43.
[2] Jankau J, Błażyńska-Spychalska A, Kubiak K, Jędrzejczak-Krzepkowska M, Pankiewicz T, Ludwicka K, et al. Bacterial Cellulose Properties Fulfilling Requirements for a Biomaterial of Choice in Reconstructive Surgery and Wound Healing. Front Bioeng Biotechnol 2022;9.
[3] Jorfi M, Foster EJ. Recent advances in nanocellulose for biomedical applications. J Appl Polym Sci 2014;132(14).
[4] Klemm D, Cranston ED, Fischer D, Gama M, Kedzior SA, Kralisch D, et al. Nanocellulose as a natural source for groundbreaking applications in materials science: Today's state. Mater Today 2018;21(7):720–48.
[5] Gorgieva S, Trček J. Bacterial Cellulose: production, Modification and Perspectives in Biomedical applications. Nanomaterials 2019;9(10).
[6] Lizundia E, Sipponen MH, Greca LG, Balakshin M, Tardy BL, Rojas OJ, et al. Multifunctional lignin-based nanocomposites and nanohybrids. Green Chem 2021;23(18):6698–760.
[7] Crouvisier-Urion K, Bodart PR, Winckler P, Raya J, Gougeon RD, Cayot P, et al. Biobased Composite Films from Chitosan and Lignin: Antioxidant activity Related to Structure and Moisture. ACS Sustain Chem Eng 2016;4(12):6371–81.
[8] Figueiredo P, Lintinen K, Hirvonen JT, Kostiainen MA, Santos HA. Properties and chemical modifications of lignin: Towards lignin-based nanomaterials for biomedical applications. Prog Mater Sci 2018;93:233–69.
[9] Galkin MV, Samec JSM. Lignin Valorization through Catalytic Lignocellulose Fractionation: a Fundamental Platform for the Future Biorefinery. ChemSusChem 2016;9(13):1544–58.
[10] Lawoko M, Samec JSM. Kraft lignin valorization: Biofuels and thermoset materials in focus. Curr Opin Green Sustainable Chem 2023;40.
[11] Melro E, Filipe A, Sousa D, Valente AJM, Romano A, Antunes FE, et al. Dissolution of kraft lignin in alkaline solutions. Int J Biol Macromol 2020;148:688–95.
[12] Melro E, Alves L, Antunes FE, Medronho B. A brief overview on lignin dissolution. J Mol Liq 2018;265:578–84.
[13] Trovagunta R, Zou T, Österberg M, Kelley SS, Lavoine N. Design strategies, properties and applications of cellulose nanomaterials-enhanced products with residual, technical or nanoscale lignin—A review. Carbohydr Polym 2021;254.
[14] Huang Z, Zhang Y, Zhang C, Yuan F, Gao H, Li Q. Lignin-based Composite Film and its Application for Agricultural Mulching. Polymers 2024;16(17).
[15] Nan N, Hu W, Wang J. Lignin-based Porous Biomaterials for Medical and Pharmaceutical applications. Biomedicines 2022;10(4).
[16] Rojo E, Peresin MS, Sampson WW, Hoeger IC, Vartiainen J, Laine J, et al. Comprehensive elucidation of the effect of residual lignin on the physical, barrier, mechanical and surface properties of nanocellulose films. Green Chem 2015;17(3):1853–66.
[17] Wang X, Wang S, Liu W, Wang S, Zhang L, Sang R, et al. Facile fabrication of cellulose composite films with excellent UV resistance and antibacterial activity. Carbohydr Polym 2019;225.
[18] Sadeghifar H, Venditti R, Jur J, Gorga RE, Pawlak JJ. Cellulose-Lignin Biodegradable and Flexible UV Protection Film. ACS Sustain Chem Eng 2016;5(1):625–31.
[19] Paulo F, Santos L. Deriving valorization of phenolic compounds from olive oil by-products for food applications through microencapsulation approaches: a comprehensive review. Crit Rev Food Sci Nutr 2020;61(6):920–45.
[20] Amara C, El Mahdi A, Akman PK, Medimagh R, Tornuk F, Khwaldia K. Use of cellulose microfibers from olive pomace to reinforce green composites for sustainable packaging applications. Food Sci Nutr 2023;11(9):5102–13.
[21] Gullón P, Gullón B, Astray G, Carpena M, Fraga-Corral M, Prieto MA, et al. Valorization of by-products from olive oil industry and added-value applications for innovative functional foods. Food Res Int 2020;137.
[22] Reyes DC, Ma Z, Romero JJ. The Antimicrobial Properties of Technical Lignins and their Derivatives—A Review. Polymers 2024;16(15).
[23] Alves C, Melro L, Fernandes M, Padrão J, Moldes D, Serra SC, et al. Plasma-treated bacterial nanocellulose-lignin composites for biomedical applications. Int J Biol Macromol 2026;338.
[24] Lee C. Targeted hyperalkalization with NaOH-loaded starch implants enhances doxorubicin efficacy in tumor treatment. Asian J Pharm Sci 2023;18(5).
[25] Chanioti S, Katsouli M, Tzia C. Novel Processes for the Extraction of Phenolic Compounds from Olive Pomace and their Protection by Encapsulation. Molecules 2021;26(6).
[26] Ma Q, Wang L, Zhai H, Ren H. Lignin dissolution model in formic acid–acetic acid–water systems based on lignin chemical structure. Int J Biol Macromol 2021;182:51–8.
[27] Su S, Kopitzky R, Tolga S, Kabasci S. Polylactide (PLA) and its Blends with Poly (butylene succinate) (PBS): a Brief Review. Polymers 2019;11(7).
[28] Jeremic S, Djokic L, Ajdačić V, Božinović N, Pavlovic V, Manojlović DD, et al. Production of bacterial nanocellulose (BNC) and its application as a solid support in transition metal catalysed cross-coupling reactions. Int J Biol Macromol 2019;129:351–60.
[29] Cielecka I, Ryngajłło M, Maniukiewicz W, Bielecki S. Highly Stretchable Bacterial Cellulose Produced by Komagataeibacter hansenii SI1. Polymers 2021;13(24).
[30] Bimmer M, Reimer M, Klingl A, Ludwig C, Zollfrank C, Liebl W, et al. Analysis of cellulose synthesis in a high-producing acetic acid bacterium Komagataeibacter hansenii. Appl Microbiol Biotechnol 2023;107(9):2947–67.
[31] Fredricks JL, Parker M, Grandgeorge P, Jimenez AM, Law E, Nelsen M, et al. The effects of temperature, pressure, and time on lignin incorporation in bacterial cellulose materials. MRS Commun 2022;12(3):394–402.
[32] Betlej I, Rybak K, Nowacka M, Antczak A, Borysiak S, Krochmal-Marczak B, et al. Structural Properties of Bacterial Cellulose Film Obtained on a Substrate Containing Sweet Potato Waste. Crystals 2022;12(9).
[33] Stanisławska A, Staroszczyk H, Szkodo M. The effect of dehydration/rehydration of bacterial nanocellulose on its tensile strength and physicochemical properties. Carbohydr Polym 2020;236.
[34] Choi SM, Rao KM, Zo SM, Shin EJ, Han SS. Bacterial Cellulose and its applications. Polymers 2022;14(6).
[35] Ashrafi Z, Lucia L, Krause W. Bioengineering tunable porosity in bacterial nanocellulose matrices. Soft Matter 2019;15(45):9359–67.
[36] Adepu S, Khandelwal M. Ex-situ modification of bacterial cellulose for immediate and sustained drug release with insights into release mechanism. Carbohydr Polym 2020;249.
[37] Hu J, Wang L, Xiao M, Chen W, Zhou M, Hu Y, et al. Insights into bacterial cellulose for adsorption and sustained-release mechanism of flavors. Food Chem: X 2025;25.
[38] Lowell S, Shields JE, Thomas MA, Thommes M. Characterization of Porous Solids and Powders. Surface Area, Pore Size and Density 2004.
[39] Gromovykh TI, Pigaleva MA, Gallyamov MO, Ivanenko IP, Ozerova KE, Kharitonova EP, et al. Structural organization of bacterial cellulose: the origin of anisotropy and layered structures. Carbohydr Polym 2020;237.
[40] Li D, Tian X, Wang Z, Guan Z, Li X, Qiao H, et al. Multifunctional adsorbent based on metal-organic framework modified bacterial cellulose/chitosan composite aerogel for high efficient removal of heavy metal ion and organic pollutant. Chem Eng J 2020;383.
[41] Zhang H, Xu X, Chen C, Chen X, Huang Y, Sun D. In situ controllable fabrication of porous bacterial cellulose. Mater Lett 2019;249:104–7.
[42] Núñez D, Cáceres R, Ide W, Varaprasad K, Oyarzún P. An ecofriendly nanocomposite of bacterial cellulose and hydroxyapatite efficiently removes lead from water. Int J Biol Macromol 2020;165:2711–20.
[43] Souza L, Antònio R, Hotza D, Carminatti C, Pineda-Vásquez T, Watzko E, et al. Lignin-incorporated bacterial nanocellulose for proton exchange membranes in microbial fuel cells. Mater Chem Phys 2023;293.
[44] Rashid T, Kait CF, Murugesan T. A "Fourier Transformed Infrared" compound Study of Lignin Recovered from a Formic Acid Process. Procedia Eng 2016;148:1312–9.
[45] Ribeiro TB, Oliveira AL, Costa C, Nunes J, Vicente AA, Pintado M. Total and Sustainable Valorisation of Olive Pomace using a Fractionation Approach. Appl Sci 2020;10(19).
[46] Mun J-S, Pe JA, Mun S-P. Chemical Characterization of Kraft Lignin Prepared from mixed Hardwoods. Molecules 2021;26(16).
[47] Nunes MA, Palmeira JD, Melo D, Machado S, Lobo JC, Costa ASG, et al. Chemical Composition and Antimicrobial activity of a New Olive Pomace Functional Ingredient. Pharmaceuticals 2021;14(9).
[48] P.J.L. Crugeira, H. Khelifa, L.M.d.S. Barreira, N. Halla, A.M. Peres, T.B. Schreiner, M.F.F. Barreiro, P. Rodrigues, Bacterial cellulose biosynthesis in the presence of raw moist olive pomace: A green sustainable approach that enhances biopolymer production and properties, Biomass and Bioenergy 197 (2025).
[49] Zimmermann KA, LeBlanc JM, Sheets KT, Fox RW, Gatenholm P. Biomimetic design of a bacterial cellulose/hydroxyapatite nanocomposite for bone healing applications. Mater Sci Eng C 2011;31(1):43–9.
[50] Sabry NW, Naeem I, Hassanien SA, Abuzalat O, Baraka A. Alkali-treatment of Lupine peels for valorizing adsorption of organic cationic pollutants from wastewater: Kinetics, isotherm, thermodynamic, regeneration, and mechanism. Next Materials 2025;8.

[51] Wang Y, Guo H, Li X, Chen X, Peng L, Zhu T, et al. Peracetic acid (PAA)-based pretreatment effectively improves medium-chain fatty acids (MCFAs) production from sewage sludge. Environ Sci Ecotechnol 2024;20.
[52] Chiang Y-C, Lee C-C, Lee H-C. Characterization of microstructure and surface properties of heat-treated PAN-and rayon-based activated carbon fibers. J Porous Mater 2006;14(2):227–37.
[53] Krishna DNG, Philip J. Review on surface-characterization applications of X-ray photoelectron spectroscopy (XPS): recent developments and challenges. Appl Surf Sci Adv 2022;12.
[54] Zhang AA, Wang ZX, Fang ZB, Li JL, Liu TF. Long-Range π–π Stacking Brings High Electron Delocalization for Enhanced Photocatalytic activity in Hydrogen-Bonded Organic Framework. Angew Chem Int Ed 2024;63(46).
[55] Gengenbach TR, Major GH, Linford MR, Easton CD. Practical guides for x-ray photoelectron spectroscopy (XPS): Interpreting the carbon 1s spectrum. J Vac Sci Technol A 2021;39(1).
[56] Sivaranjini B, Mangaiyarkarasi R, Ganesh V, Umadevi S. Vertical Alignment of Liquid Crystals over a Functionalized Flexible Substrate. Sci Rep 2018;8(1).
[57] Padrão J, Ribeiro S, Lanceros-Méndez S, Rodrigues LR, Dourado F. Effect of bacterial nanocellulose binding on the bactericidal activity of bovine lactoferrin. Heliyon 2020;6(7).
[58] Jacobs TW, Dillon JT, Cohen DJ, Boyan BD, Schwartz Z. Different Methods to Modify the Hydrophilicity of Titanium Implants with Biomimetic Surface Topography to Induce Variable responses in Bone Marrow Stromal Cells. Biomimetics 2024;9(4).
[59] Lavrič G, Oberlintner A, Filipova I, Novak U, Likozar B, Vrabič-Brodnjak U. Functional Nanocellulose, Alginate and Chitosan Nanocomposites Designed as active Film packaging Materials. Polymers 2021;13(15).
[60] Chen S-Q, Cao X, Li Z, Zhu J, Li L. Effect of lyophilization on the bacterial cellulose produced by different Komagataeibacter strains to adsorb epicatechin. Carbohydr Polym 2020;246.
[61] Guo L, Li M, Xu Q, Jin L, Wang Y. Bio-based films with high antioxidant and improved water-resistant properties from cellulose nanofibres and lignin nanoparticles. Int J Biol Macromol 2023;227:365–72.
[62] Ruwoldt J, Blindheim FH, Chinga-Carrasco G. Functional surfaces, films, and coatings with lignin – a critical review. RSC Adv 2023;13(18):12529–53.
[63] Lin C-F, Karlsson O, Myronycheva O, Das O, Mensah RA, Mantanis GI, et al. Phosphorylated and carbamylated Kraft lignin for improving fire- and biological-resistance of Scots pine wood. Int J Biol Macromol 2024;276.
[64] Mohamad S, Abdullah LC, Jamari SS, Al Edrus SSO, Aung MM, Mohamad SFS. Influence of drying method on the crystal structure and thermal property of oil palm frond juice-based bacterial cellulose. J Mater Sci 2022;57(2):1462–73.
[65] Sánchez-Ávila N, Cardarelli A, Carmona-Cabello M, Dorado MP, Pinzi S, Barbanera M. Kinetic and thermodynamic behavior of co-pyrolysis of olive pomace and thermoplastic waste via thermogravimetric analysis. Renew Energy 2024;230.
[66] Parit M, Du H, Zhang X, Jiang Z. Flexible, Transparent, UV-Protecting, Water-Resistant Nanocomposite Films based on polyvinyl Alcohol and Kraft Lignin-Grafted Cellulose Nanofibers. ACS Appl Polym Mater 2022;4(5):3587–97.
[67] Ojeda JJ, Romero-González ME, Bachmann RT, Edyvean RGJ, Banwart SA. Characterization of the Cell Surface and Cell Wall Chemistry of Drinking Water Bacteria by Combining XPS. FTIR Spectroscopy, Modeling, and Potentiometric Titrations, Langmuir 2008;24(8):4032–40.
[68] Chunshom N, Chuysinuan P, Techasakul S, Ummartyotin S. Dried-state bacterial cellulose (Acetobacter xylinum) and polyvinyl-alcohol-based hydrogel: an approach to a personal care material. J Sci: Adv Mater Devices 2018;3(3):296–302.
[69] Bodea IM, Beteg FI, Pop CR, David AP, Dudescu MC, Vilău C, et al. Optimization of Moist and Oven-Dried Bacterial Cellulose Production for Functional Properties. Polymers 2021;13(13).
[70] Jantarat C, Muenraya P, Srivaro S, Nawakitrangsan A, Promsornpason K. Comparison of drug release behavior of bacterial cellulose loaded with ibuprofen and propranolol hydrochloride. RSC Adv 2021;11(59):37354–65.
[71] Bary EMA, Fekri A, Soliman YA, Harmal AN. Characterisation and swelling–deswelling properties of superabsorbent membranes made of PVA and cellulose nanocrystals. Int J Environ Stud 2018;76(1):118–35.
[72] Chunshom N, Chuysinuan P, Thanyacharoen T, Techasakul S, Ummartyotin S. Development of gallic acid/cyclodextrin inclusion complex in freeze-dried bacterial cellulose and poly (vinyl alcohol) hydrogel: Controlled-release characteristic and antioxidant properties. Mater Chem Phys 2019;232:294–300.
[73] Roche S, D'Ippolito G, Gomez LA, Bouckenooghe T, Lehmann S, Montero-Menei CN, et al. Comparative analysis of protein expression of three stem cell populations: Models of cytokine delivery system in vivo. Int J Pharm 2013;440(1):72–82.
[74] Costa P, Sousa Lobo JM. Evaluation of Mathematical Models describing Drug Release from Estradiol Transdermal Systems. Drug Dev Ind Pharm 2003;29(1):89–97.
[75] Zhang Y, Huo M, Zhou J, Zou A, Li W, Yao C, et al. DDSolver: an Add-In program for Modeling and Comparison of Drug Dissolution Profiles. AAPS J 2010;12(3):263–71.
[76] Costa L, Carvalho AF, Fernandes AJS, Campos T, Dourado N, Costa FM, et al. Bacterial nanocellulose as a simple and tailorable platform for controlled drug release. Int J Pharm 2024;663.
[77] Ribeiro AI, Vieira B, Dantas D, Silva B, Pinto E, Cerqueira F, et al. Synergistic Antimicrobial activity of Silver Nanoparticles with an Emergent Class of Azoimidazoles. Pharmaceutics 2023;15(3).
[78] Sunthornvarabhas J, Liengprayoon S, Suwonsichon T. Antimicrobial kinetic activities of lignin from sugarcane bagasse for textile product. Ind Crop Prod 2017;109:857–61.
[79] Dong X, Dong M, Lu Y, Turley A, Jin T, Wu C. Antimicrobial and antioxidant activities of lignin from residue of corn stover to ethanol production. Ind Crop Prod 2011;34(3):1629–34.
[80] Sugiarto S, Leow Y, Tan CL, Wang G, Kai D. How far is Lignin from being a biomedical material? Bioact Mater 2022;8:71–94.
[81] Domínguez-Robles J, Cárcamo-Martínez Á, Stewart SA, Donnelly RF, Larrañeta E, Borrega M. Lignin for pharmaceutical and biomedical applications – could this become a reality? Sustain Chem Pharm 2020;18.
[82] Vieira B, Padrão J, Alves C, Silva C, Vilaça H, Zille A. Enhancing Functionalization of Health Care Textiles with Gold Nanoparticle-Loaded Hydroxyapatite Composites. Nanomaterials 2023;13(11).
[83] Jiji S, Udhayakumar S, Maharajan K, Rose C, Muralidharan C, Kadirvelu K. Bacterial cellulose matrix with in situ impregnation of silver nanoparticles via catecholic redox chemistry for third degree burn wound healing. Carbohydr Polym 2020;245.
[84] Yang W, Fortunati E, Dominici F, Giovanale G, Mazzaglia A, Balestra GM, et al. Effect of cellulose and lignin on disintegration, antimicrobial and antioxidant properties of PLA active films. Int J Biol Macromol 2016;89:360–8.
[85] Lammi S, Gastaldi E, Gaubiac F, Angellier-Coussy H. How olive pomace can be valorized as fillers to tune the biodegradation of PHBV based composites. Polym Degrad Stab 2019;166:325–33.
[86] Ghanbari Shendi E, Sivri Ozay D, Ozkaya MT, Ustunel NF. Changes occurring in chemical composition and oxidative stability of virgin olive oil during storage. Ocl 2018;25(6).
[87] Mulinacci N, Ieri F, Ignesti G, Romani A, Michelozzi M, Creti D, et al. The freezing process helps to preserve the quality of extra virgin olive oil over time: a case study up to 18months. Food Res Int 2013;54(2):2008–15.
[88] Cunliffe AJ, Askew PD, Stephan I, Iredale G, Cosemans P, Simmons LM, et al. How do we Determine the Efficacy of an Antibacterial Surface? a Review of Standardised Antibacterial Material Testing Methods. Antibiotics 2021;10(9).
[89] Madureira J, Gonçalves I, Cardoso J, Dias MI, Santos PMP, Margaça FMA, et al. Effects of Electron Beam Radiation on the Phenolic Composition and Bioactive Properties of Olive Pomace Extracts. Antioxidants 2024;13(5).
[90] Yang J, Liu C, Sun H, Liu Y, Liu Z, Zhang D, et al. The progress in titanium alloys used as biomedical implants: from the view of reactive oxygen species. Front Bioeng Biotechnol 2022;10.
[91] Lourençon TV, de Lima GG, Ribeiro CSP, Hansel FA, Maciel GM, da Silva K, et al. Antioxidant, antibacterial and antitumoural activities of kraft lignin from hardwood fractionated by acid precipitation. Int J Biol Macromol 2021;166:1535–42.
[92] Črešnar KP, Zamboulis A, Bikiaris DN, Aulova A, Zemljič LF. Kraft Lignin/Tannin as a potential Accelerator of Antioxidant and Antibacterial Properties in an active Thermoplastic Polyester-based Multifunctional Material. Polymers 2022;14(8).
[93] Quero J, Ballesteros LF, Ferreira-Santos P, Velderrain-Rodriguez GR, Rocha CMR, Pereira RN, et al. Unveiling the Antioxidant Therapeutic Functionality of Sustainable Olive Pomace active Ingredients. Antioxidants 2022;11(5).
[94] Cabañas-Romero LV, Valls C, Valenzuela SV, Roncero MB, Pastor FIJ, Diaz P, et al. Bacterial Cellulose–Chitosan Paper with Antimicrobial and Antioxidant Activities. Biomacromolecules 2020;21(4):1568–77.
[95] Buruaga-Ramiro C, Valenzuela SV, Valls C, Roncero MB, Pastor FIJ, Díaz P, et al. Development of an antimicrobial bioactive paper made from bacterial cellulose. Int J Biol Macromol 2020;158:587–94.
[96] Gómez-Cruz I, del Mar Contreras M, Romero I, Castro E. A biorefinery approach to obtain antioxidants, lignin and sugars from exhausted olive pomace. J Ind Eng Chem 2021;96:356–63.